Histone concentration regulates the cell cycle and transcription in early development

Henry Wilky[1], Sudarshan Chari[1], Jayalakshmi Govindan and Amanda A. Amodeo*

Lewis-Sigler Institute for Integrative Genomics, Princeton University
[1]These authors contributed equally
*Corresponding author: Amanda Amodeo (aamodeo@princeton.edu)

Keywords:
Chromatin; Maternal to zygotic transition; MZT; Mid-blastula transition; MBT; Zygotic genome activation; ZGA; nuclear cytoplasmic ratio; cell cycle

Summary Statement:
Overexpression or knockdown of histones results in delayed or advanced cell cycle slowing and transcriptional activation at the mid-blastula transition respectively. Differentially expressed genes are associated with specific chromatin features.

Abstract:
The early embryos of many animals including flies, fish, and frogs have unusually rapid cell cycles and delayed onset of transcription. These divisions are dependent on maternally supplied RNAs and proteins including histones. Previous work suggests that the pool size of maternally provided histones can alter the timing of zygotic genome activation (ZGA) in frogs and fish. Here, we examine the effects of under and overexpression of maternal histones in *Drosophila* embryogenesis. Decreasing histone concentration advances zygotic transcription, cell cycle elongation, Chk1 activation, and gastrulation. Conversely, increasing histone concentration delays transcription and results in an additional nuclear cycle before gastrulation. Numerous zygotic transcripts are sensitive to histone concentration, and the promoters of histone sensitive genes are associated with specific chromatin features linked to increased histone turnover. These include enrichment of the pioneer transcription factor Zelda and lack of SIN3A and associated histone deacetylases. Our findings uncover a critical regulatory role for histone concentrations in ZGA of *Drosophila*.

Introduction:
Upon fertilization the embryo must produce enough cells to pattern a functioning organism. Many species accomplish this by undergoing rapid cleavage divisions with little transcription. This is followed by zygotic genome activation (ZGA) (Tadros and Lipshitz, 2009; Vastenhouw et al., 2019; Harrison and Eisen 2015; Blythe and Wieschaus 2015a). In many organisms ZGA coincides with cell cycle slowing which precedes the onset of morphogenesis during a period called the Mid-Blastula Transition (MBT) (Newport and Kirschner, 1982a, 1982b). In *Drosophila,* the initial divisions are further shortened through omission of cytokinesis resulting in a syncytium for the first 13 nuclear cycles (NCs), which becomes cellularized when the cycle slows in NC14 (Foe and Alberts, 1983). This switch from transcriptionally silenced, rapid nuclear cycles to transcriptionally active, slower cycles is accompanied by changes in the chromatin landscape. In *Drosophila*, transcription factors bind their consensus sequences (Harrison et al., 2010, 2011; Liang et al., 2008; Driever and Nüsslein-Volhard, 1989), RNA polymerase is gradually recruited to sites of transcription (Gaertner et al., 2012; Chen et al., 2013; Blythe and Wieschaus, 2015b), and nucleosome free regions open on promoters (Li et al., 2014; Blythe and Wieschaus, 2016). At a larger scale, the genome becomes folded into topologically associated domains, and heterochromatin is differentiated from euchromatin for the first time (Hug et al., 2017; Shermoen et al., 2010; Seller et al., 2018).

The early divisions are fueled by maternally supplied RNAs, proteins, and metabolites (Newport and Kirschner, 1982a, 1982b; Vastag et al., 2011; Song et al., 2017; Collart et al., 2013; Djabrayan et al., 2019; Liu et al., 2019). Chromatin components, including core histones, are loaded in vast excess of what is required for the first divisions (Horard and Loppin, 2015; Adamson and Woodland, 1974; Woodland and Adamson, 1977; Shindo and Amodeo, 2019). In *Drosophila*, maternal histone stores are sufficient for progression through the MBT, but zygotic histone production is required for progression past the first post-MBT cell cycle (Gunesdogan et al., 2010, 2014; Zhang et al., 2018). It has been suggested that overabundant histones compete with transcription factors for DNA binding to repress transcription in the early cycles (Almouzni et al., 1990,1991; Prioleau et al., 1994; Almouzni and Wolffe, 1995; Amodeo et al., 2015; Joseph et al., 2017). Indeed, pioneer transcription factors are required to evict nucleosomes at ZGA and altering the concentration of core histones in the early embryos of both *Xenopus* and zebrafish can modulate the timing of ZGA (Liang et al., 2008; Harrison et al., 2010, 2011; Lee et al., 2013; Leichsenring et al., 2013; Amodeo et al., 2015; Joseph et al., 2017). Although the loss of embryonic linker histone H1 has been implicated in timing *Drosophila* ZGA, the role of core histones has not been well characterized (Pèrez-Montero et al., 2013).

Here, we examine the effect of histone concentration on the MBT in *Drosophila*. We manipulate maternally deposited histone concentration and examine the effects on cell cycle and transcription. Histone reduction results in slower and fewer nuclear cycles, while histone increase results in additional cycles. We demonstrate that cell cycle changes correspond to large changes in zygotic transcription and maternal mRNA degradation consistent with alterations to ZGA. We identify a subset of transcripts as directly histone sensitive. The promoters of histone sensitive genes are enriched for the pioneer transcription factor Zelda (ZLD) and the absence of the transcriptional repressor SIN3A and associated histone deacetylases (HDACs). Together these results demonstrate a direct role for histone concentrations in regulating the MBT, provide a list of transcripts that are both directly and indirectly sensitive to histone concentration, and identify the chromatin features that underlie direct histone sensitivity.

Results:

Histone concentration regulates the timing of the MBT

To understand the effects of histone concentration on the MBT we reduced maternally supplied histones by downregulating a critical histone regulator, *Stem Loop Binding Protein* (*Slbp*) (Sullivan et al., 2001; Dominski et al., 2002; Lanzotti et al., 2002; Iampietro et al., 2014; Lefebvre et al., 2017; He et al., 2018) via maternally driven RNAi (Perkins et al, 2015). Under these conditions, histone H2B was reduced by ~50% and H3 by ~60% at the MBT (Figure S1A). Approximately 50% of embryos laid by *Slbp* RNAi mothers (henceforth *Slbp* embryos) that form a successful blastoderm do not undergo the final division and attempt gastrulation in NC13 (Figure 1A, Movie 1). Another ~30% exhibit an intermediate phenotype of partial arrest with only part of the embryo entering NC14 (Movie 2). A minority of *Slbp* embryos begin gastrulation with all nuclei in NC14. NC12 duration was predictive of NC13 arrest with NC12 being an average of ~5 minutes longer in *Slbp* embryos that went on to arrest compared to those that did not arrest ($p=0.0034035$) (Figure 1C, Table S1, see methods).

We first detected cellularization in WT embryos ~20 minutes into NC14. Partially arrested *Slbp* embryos also began cellularization ~20 minutes into NC14 with nuclei arrested in NC13 waiting until the remainder of the embryo has entered NC14 to cellularize. Fully arrested embryos began cellularization ~20 minutes into NC13 initiating cellularization one cycle early and ~20 minutes earlier in overall developmental time than WT. Despite their reduced cell number, these embryos form mitotic domains and gastrulate without obvious defects, however they die before hatching (Figure S2A and B).

To examine the effects of increased histone concentration on developmental timing we monitored cell cycle progression in embryos from *abnormal oocyte* (*abo*) mutant mothers (henceforth *abo* embryos). *abo* is a histone locus specific transcription factor whose knockdown increases the production of replication coupled histones, particularly H2A and H2B (Berloco et al., 2001). We found that *abo* increased H2B by ~90% while total (combined replication-coupled and replication-independent) H3 was not affected in NC14 embryos (Figure S1B). Approximately 60% of *abo* embryos display fertilization defects or catastrophic early nuclear divisions (Table S1, Tomkiel et al., 1995). Of *abo* embryos that form a functioning blastoderm, ~6% undergo a complete extra nuclear division before gastrulating in NC15 while ~4% undergo a partial extra nuclear division (Figure 1B, Movie 3, Movie 4). Embryos from *abo* mothers that complete total extra divisions have faster NC14s in which they do not cellularize and spend 40-60 minutes in NC15 before gastrulating (Figure 1D). This suggests an alteration of the normal transcription-dependent developmental program. In some cases, the cell cycle program and transcriptional program may be decoupled evidenced by the fact that some *abo* embryos attempt to gastrulate while still in the process of division. *abo* embryos that undergo extra divisions exhibit a range of gastrulation defects including expanded mitotic domains and ectopic furrow formation (Figure S2A and C, Movie 3, Movie 4).

Since alterations in histone levels can both decrease and increase the number of divisions before cell cycle slowing we reasoned that histone levels might affect activation of checkpoint kinase 1 (Chk1/grp), which is required for cell cycle slowing at the MBT (Fogarty et al., 1994, 1997; Sibon et al., 1997, 1999). To test this, we crossed a fluorescent biosensor of Chk1 activity into the *Slbp* background (Deneke et al., 2016). We found that even in *Slbp* embryos that did not undergo early gastrulation, Chk1 activity was higher than in WT, consistent with the lengthened cell cycle (Figure 1E). This result indicates that the observed cell cycle phenotypes in the histone manipulated embryos are likely mediated through changes in Chk1 activity.

Low histone concentration advances and high histone concentration delays ZGA
Since cellularization and gastrulation require zygotic transcription we suspected that embryos with altered development likely have altered gene expression. We performed single-embryo RNA-seq on staged *Slbp* embryos that remained in NC13 for greater than 30 minutes (Figure 2A). We compared these to either nuclear cycle matched (NC13) or time matched (NC14) WT embryos. To control for maternal effects of *Slbp* RNAi, we collected pre-blastoderm stage WT and *Slbp* embryos. We found that the *Slbp* embryos undergo ZGA one nuclear cycle earlier than WT. We identify ~5000 genes that are differentially expressed (see methods for details) between *Slbp* and WT NC13 with ~60% being upregulated (Figure 2B, Table S2-5). The upregulated genes have largely previously been identified as new zygotic transcripts including cell cycle regulators like *fruhstart* (*frs*/*Z600*) and signaling molecules like *four-jointed* (*fj*), while the downregulated genes are enriched for maternally degraded transcripts (Figure 2C-D, Table S6) (Lott et al., 2011; De Renzis et al., 2007). We believe this represents a coherent change in ZGA timing instead of global transcription dysregulation, since 98% of the genes that are overexpressed in *Slbp* are expressed before the end of NC14 in our control or previously published datasets (Table S20) (Lott et al., 2011). Indeed, the transcriptomes of histone depleted embryos that stopped in NC13 are more similar to WT NC14 than WT NC13 which suggests a role for cell cycle elongation in ZGA (Figure S3A, Yuan et al., 2016). Nonetheless, ~1500 genes are differentially expressed between *Slbp* NC13 and WT NC14 without accounting for differences in ploidy. Of these, the majority of the ~1000 overexpressed genes are again associated with zygotic transcription and downregulated genes associated with maternal products (Figure S3E, Table S2-6, S14, and S15). Thus, ZGA is even further accelerated in the histone knock-down than can be explained by purely time alone.

Since ZGA is accelerated by histone depletion, we asked whether ZGA would be delayed in the histone overexpression mutant. We performed RNA-seq on pools of *abo* and WT embryos collected 15-30 minutes into NC14 (Figure 3A). We identify >1000 genes that are differentially expressed between *abo* and WT, with approximately equal numbers of genes up and down regulated (Figure 3B and Table S2 and S7-9). As expected, the downregulated genes in *abo* are enriched for previously identified zygotically expressed transcripts (Lott et al., 2011; De Renzis et al., 2007) (Figure 3D, Table S6 and S14), and upregulated transcripts are enriched for maternally deposited genes. Thus, histone overexpression delays the onset of ZGA.

Zygotic genes whose transcription is upregulated by histone depletion and downregulated by histone overexpression contains many important developmental and cell cycle regulators including: *frs*, *hairy (h)*, *fushi tarazu* (*ftz*) and *odd-paired* (*odd*) (Figure 2C and 3C, Table S4, S7, and S8). Conversely, the maternally degraded transcripts that are destabilized by histone depletion and stabilized by histone overexpression include several cell cycle regulators such as *Cyclin B* (*CycB*), *string* (*Stg*), and *Myt1* (Table S4, S7, and S8). Therefore, histone concentration can modulate the expression and stability of specific cell cycle regulators, which may contribute to the onset of MBT.

Since histone concentration has previously been implicated in sensing the nuclear-cytoplasmic (N/C) ratio (Amodeo et al., 2015), we compared the genes that are changed in both the histone under and overexpression embryos to those that had been previously found to be dependent on either the N/C ratio or developmental time (Lu et al., 2009). Both previously identified N/C ratio dependent and time dependent genes (Lu et al., 2009) followed the same general trends as the total zygotic gene sets (De Renzis et al., 2007), indicating that histone availability cannot explain these previous classifications (Figure S6 and Table S6).

Next, we sought to disentangle the effects of cell cycle length from transcription in the histone overexpression mutant. We performed single-embryo time-course RNA-seq on *abo* and WT embryos 3 collected minutes before mitosis of NC10-NC13 and 3 minutes into NC14 (Figure 3E). Additionally, we collected unfertilized embryos (henceforth, "NC0") of both genotypes to control for differences in maternal contribution. Even with a stringent selection process that accounted for cell cycle time and embryo health (see Materials and Methods, Figure S5A and B, Tables S2 and S10-13), we identify a small set of robustly upregulated (179) and downregulated (260) genes across NC10-NC14. Of the newly transcribed genes, we detect 111 genes whose transcription is delayed including *frs* (Figure 3F) and only 37 that are upregulated (Table S14). We confirmed these results by qPCR (Figure 3G). When compared with previous datasets zygotic genes tend to be underexpressed as was the case for the pooled *abo* dataset, however the majority of these enrichments are not statistically significant (Figure S6D). Nonetheless the majority of these underexpressed genes are expressed during NC14 in WT (Lott et al., 2011) (Figure S7). This gene set in combination with the time matched *Slbp* comparison enables further examination of the chromatin features that underlie histone sensitivity for transcription independent of cell cycle changes.

Histone sensitive genes contain specific chromatin features around the TSS

To identify chromatin features associated with histone sensitivity, we compared the presence of 143 ModENCODE chromatin signals near the transcriptional start site (TSS +/- 500bp) of genes whose expression was altered by changes in histone concentration independent of cell cycle time (Figures S3, Figure 3E and Figure 4A). We found a clear pattern of unique chromatin features for the histone sensitive genes as compared to all newly transcribed genes that is highly similar between the histone over- and under-expression experiments (Figure 4B, Table S17 and S18). The pioneer transcription factor ZLD, known to be important for nucleosome eviction during ZGA, is enriched in the promoters of histone sensitive genes. Insulator proteins such as BEAF-32 and CP190 are depleted in histone sensitive genes. Chen et al., 2013; Li et al., 2014). Promoters of histone sensitive genes also show a strong reduction for SIN3A, a transcriptional repressor associated with cell cycle regulation (Pile et al., 2002; David et al., 2008). SIN3A is known to recruit histone deacetylases (HDACs) to TSSs and almost all HDACs also show significant de-enrichment at the TSSs of histone sensitive genes (Kadosh and Struhl, 1998; Silverstein and Ekwall, 2005). Taken together these marks make up a unique chromatin signature that may sensitize a locus to changes in histone concentration as is likely for pioneer factors such as ZLD. Other aspects of this signature may indicate that these genes are subsequently subject to later developmental regulation as indicated by H3K4me3 and H3K27me3 (Li et al., 2014; Chen et al., 2013).

Discussion:

In this study, we have demonstrated that histone concentration regulates the timing of the MBT in *Drosophila*, resulting in both early gastrulation and extra pre-MBT divisions from histone reduction and increase respectively. Histone concentration also regulates ZGA. Thousands of genes are prematurely transcribed in histone depleted and hundreds of genes delayed in histone overexpressing embryos. The majority of these genes appear downstream of changes in cell cycle duration suggesting a model where histones directly regulate cell cycle progression. In other cell types, histones loss halts the cell cycle via accumulation of DNA damage and stalled replication forks (Ye et al., 2003; Prado and Aguilera, 2004; Groth et al., 2007; Gunjan and Verreault, 2003). In the early embryo, changes in histone availability may similarly create replication stress to directly or indirectly activate Chk1 as we have shown. Chk1 in turn would inhibit Cdc25/String and/or Twine to slow the cell cycle (Di Talia et al., 2013; Farrell & O'Farrell, 2013; Deneke et al., 2016; Royou et al., 2008; Fasulo et al., 2012; Price et al., 2000; Ji et al., 2004; Stumpff et al., 2004; Shimuta et al., 2002). This mechanism is supported by previous observations that loss of zygotic histones causes the down regulation of Cdc25/String in the first post-MBT cell cycle

(Gunesdogan et al., 2014). In this case, the observed transcriptional changes would be independent or downstream of the altered cell cycle.

Alternatively, direct changes in transcription downstream of histone availability may feed into the cell cycle. In bulk, histone sensitive transcripts might underlie the replication stress that has been previously proposed to slow the cell cycle at the MBT (Blythe and Wieschaus, 2015b). Consistent with this, the cell cycle lengthening and partial arrest phenotypes observed in mutant RNA Pol II embryos occur at a similar frequency to those we observe as the result of histone depletion (Sung et al., 2013). Another possibility is that specific histone sensitive transcripts are responsible for cell cycle elongation. One promising candidate for a histone sensitive cell cycle regulator is the N/C ratio sensitive CDK inhibitor *frs*, since zygotic transcription of *frs* plays a critical role in stopping the cell cycle at the MBT (Grosshans et al., 2003). In contrast, *tribbles*, an N/C ratio dependent inhibitor of Cdc25/Twine that has also been implicated in cell cycle slowing, does not show a consistent response between histone perturbations (Farrell & O'Farrell, 2013). In this previously proposed model, maternal histone stores may compete with pioneer transcription factors to set the timing of transcription initiation (Amodeo et al., 2015; Joseph et al., 2017). Indeed, the central *Drosophila* pioneer transcription factor ZLD is enriched at the promoters of histone sensitive genes. Moreover, we have identified a broader set of chromatin features which may sensitize individual loci to changes in histone concentrations. These include less obvious candidates for global early transcriptional regulators like SIN3A, HDACs, and class I insulator proteins that may protect transcripts from changes in histone concentrations. Our work highlights the importance of histone concentration in regulating the timing of MBT and provides evidence that promoters of histone sensitive genes possess a unique chromatin signature. However, future studies will be required to isolate the specific downstream effectors that respond to changes in histone concentrations in the early embryo.

Materials and Methods:

***Drosophila* stocks and genetic crosses**

Slbp RNAi (BSC: 51171), *abo*1 (BSC: 2525), OvoD/bTub85 (BSC: 2149), and nls-RFP (BSC: 31418) lines were obtained from the Bloomington *Drosophila* Stock Center (NIH P40OD018537). Oregon-R (Ore-R) and P(mat-tub-Gal4)mat67; P(mat-tub-Gal4)mat15 were a gift from Eric Wieschaus (Princeton University). The Chk1 localization sensor was a gift from Stefano Di Talia (Duke University). All fly stocks were maintained through standard methods at 25°C unless otherwise specified and grown on a standard cornmeal media. *Slbp* embryos were produced by crossing nls-RFP; P(mat-tub-Gal4)mat67; P(mat-tub-Gal4)mat15 driver virgin females to UAS-*Slbp* RNAi males at 18°C. The resulting female progeny were placed into cups with Ore-R males at 18°C and their embryos used for experiments. Wild-type for *Slbp* experiments was nls-RFP; P(mat-tub-Gal4)mat67; P(mat-tub-Gal4)mat15 driver virgin females crossed to Ore-R males at 18°C. The resulting female progeny were placed into cups with Ore-R males at 18°C, and their embryos used as WT controls for *Slbp* experiments. *abo* embryos were produced by collecting nls-RFP; abo^{1} homozygous females from a nls-RFP; abo^{1}/SM1 stock line. Females were placed into cups with Ore-R males at 25°C, and their embryos were used for experiments. For *abo* control experiments nls-RFP females were collected and placed into cups with Ore-R males at 25°C, and their embryos were used as wild-type. We found no significant deviations in cell cycle duration between wild-type embryos laid at 18°C or 25°C once imaging began at 22°C indicating that any temperature-dependent effects on the cell cycle were mitigated by imaging at a constant temperature. Unfertilized embryos were collected from crossing nls-RFP; + ; and nls-RFP; *abo*1 ; homozygous virgin females to st1 βTub85DD ss1 es/TM3, Sb1 males derived from the OvoD/bTub85 (BSC: 2149). *Slbp* Chk1 sensor embryos were produced by crossing nls-RFP;Pmat-tub-Gal4)mat67; P(mat-tub-Gal4)mat15 driver virgin females to y,w ; UAS-*Slbp*

RNAi ; Cdc25C[183-251]-EGFP males at 18°C. The resulting female progeny were placed into cups with Ore-R males at 18°C and their embryos used for experiments. Wild-type for Chk1 sensor experiments was nls-RFP; P(mat-tub-Gal4)mat67; P(mat-tub-Gal4)mat15 driver virgin females crossed to y,w ; ; Cdc25C[183-251]-EGFP males at 18°C. The resulting female progeny were placed into cups with y,w males at 18°C, and their embryos used as WT controls for *Slbp* Chk1 experiments.

Microscopy
Embryos were dechorionated with 4% sodium hypochlorite and mounted on a 35mm coverslip dish (MatTek) and covered with water. Cell cycle observations and RNA collections for *Slbp* and *abo* embryos were taken at 22°C using a Nikon Ti-E spinning disk confocal microscope with a 20x1.3 NA air objective at 60s/frame acquisition (1022 x 1500 pixel area). Wild-type and *Slbp* embryos expressing a Chk1 activity sensor were acquired at 24°C using a Nikon A1R-Si HD confocal microscope with a 60x1.4 NA oil objective at 20s/frame (500 x 248 pixel area). Images were processed with Nikon NIS-Elements and FIJI.

Cell cycle analysis
The duration of a nuclear cycle was calculated from the number of frames between nuclear envelope breakdown in at least 50% of the nuclei in the embryo to 50% nuclear envelope breakdown in the next nuclear cycle. Gastrulation was determined when multiple cells began movement away from the single tissue sheet.

Statistical significance for nuclear cycle duration between WT and *Slbp* embryos for each nuclear cycle was determined by two-way ANOVA performed using R (3.4). Statistical parameters such as sample numbers, mean, and adjusted p-value for multiple comparisons are included as follows: For NC12 - *Slbp* early n=7, mean=23.9 min; WT n=6, mean=16.7 min; p=0.0000583. *Slbp* early n=7, mean=23.9 min; *Slbp* normal n=4, mean=19.5 min; p=0.0034035. *Slbp* normal n=4, mean=19.5 min; WT n=6, mean=16.7 min; p=0.1308121. For NC13 - *Slbp* early n=4, mean=86.8 min; WT n=7, mean=25.6 min; p<0.0000001. *Slbp* normal n=4, mean=33.3 min; WT n=7, mean=25.6 min; p=0.0056589. *Slbp* early n=4, mean=86.8 min, *Slbp* normal n=4, mean=33.3 min; p<0.0000001.

Chk1 activity measurement
Wild-type and *Slbp* embryos were imaged from NC11 to NC13 mitosis with a Chk1 activity sensor (Deneke et al., 2016). Chk1 activity was determined from the cytoplasmic-to-nuclear intensity ratio of the Chk1 localization sensor in 150 x 75 pixel area. Nuclear signal was taken from segmented nuclei eroded by 2 pixels to ensure nuclear signal was analyzed. Cytoplasmic signal was taken from inverted nuclear masks dilated by 2 pixels. Four embryos per genotype were analyzed.

Single embryo qPCR
cDNA from RNA isolated from single embryos collected 3 minutes into NC14 was made with random primer mix using ProtoScript First Strand cDNA Synthesis Kit following manufacturer's protocol (NEB, E6560L). qPCR was conducted on an ABI ViiA7 using the FG Taqman GEX master mix (ThermoFisher, 4369016) and the following gene expression assays: *frs* (DM01822845; VIC) normalized to RPL32 (DM02151887; FAM).

Western Blotting
For western blotting, protein extracts were collected from wild-type, *Slbp*, and *abo* embryos 55 minutes after pole bud formation corresponding to early NC14 in the wild-type and individually staged-confirmed by halocarbon oil (Sigma, H8773). Embryos were washed with DI water, dechorionated with 4% sodium hypochlorite, washed again with DI water, then lysed in ice-cold embryo lysis buffer (as per Gunesdogan et al., 2014). Laemmli buffer (Bio-Rad Laboratories, 1610737) was added to each sample, and they were incubated at 95°C for 10 minutes. Five embryos were collected per sample. Proteins were separated on a TGX

12% acrylamide gel (Bio-Rad Laboratories), stain free dye was crosslinked under UV for 1 min, and transferred to a low fluorescence PVDF membrane. Membranes were incubated overnight in rabbit anti-H3 antibody (1:2,000; Abcam: ab1791) and mouse anti-H2B antibody (1:2000, Abcam: ab52484), washed, and then incubated for a minimum of 1 h in Alexa Fluor 647-conjugated goat anti-rabbit IgG antibody (1:2,500; Invitrogen: A-21244) and/or Alexa Fluor 488-conjugated goat anti-mouse IgG antibody (1:2,500; Invitrogen: A-11001). Fluorescence was detected using a gel imager (Bio-Rad ChemiDoc MP) and quantified in Image Lab. H2B and H3 signal were normalized to total protein using the bright, ~45 kDa band in the Stain-Free channel which corresponds to vitellogenin. For the *Slbp* and WT comparison, the normalized H2B and H3 protein concentrations were averaged for each genotype and the average WT concentration for each protein was scaled to a value of 1. Error was calculated using a linear model in R (lm in base R) to account for gel differences and extracted the mean Genotype effects and the associated standard error. (Figure S1A,B).

RNA collection - single embryo and pooled
Input RNA for RNA-Seq and qPCR were collected from individual and pooled embryos laid by tightly staged WT (as defined above), *abo* homozygous, and *Slbp* RNAi mothers gathered from apple juice agar plates with yeast. Individual embryos were placed into an RNAse free tube, were lysed, added 100ul lysis buffer (Applied Biosystems, KIT0214), flash-frozen in liquid nitrogen, then stored in -80°C. Pooled embryos were placed in 100 ul RNAlater (Invitrogen, AM7020) and stored at 4°C. When enough embryos were collected RNAlater was removed, and embryos were processed as above. See Supplementary Materials and Methods for further details on RNA collections.

cDNA Library Preparation and Sequencing
The integrity of total RNA samples was assessed on Bioanalyzer 2100 using RNA 6000 Pico chip (Agilent Technologies).

Single WT and *Slbp* embryos:
For single embryo WT and *Slbp* RNA samples, additional ribosomal RNA depletion was applied prior to the Smart-seq2 library preparation using the Ribo-Zero rRNA Removal (Human, Mouse, Rat) Kit (Illumina, MRZH11124). The cDNA samples, RNA-seq and libraries were examined on the Bioanalyzer (Agilent Technologies). DNA HS chips for size distribution and quantified by Qubit fluorometer (Invitrogen). Different DNA barcodes were added to each sequencing library, and the libraries to be sequenced together were pooled at equal molar amount. The RNA-seq libraries were sequenced on Illumina HiSeq 2500 Rapid flow-cells as single-end 75nt reads, following the standard Illumina protocol. Raw sequencing reads were filtered by Illumina HiSeq Control Software and only the Pass-Filter reads were used for further analysis.

Single, time course WT and *abo* embryos:
For RNA samples from single, time-course WT and *abo* embryos, the poly-A containing RNA transcripts were converted to cDNA using oligo-dT adaptor and further amplified by PCR following the Smart-seq2 method (Picelli et al, 2014). Illumina sequencing libraries were made from the amplified cDNA samples using the Nextera DNA library prep kit (Illumina, FC-121-1031).

Pooled WT and *abo* embryos:
For RNA samples from pooled WT and *abo* embryos. Poly-A containing RNA transcripts were enriched using oligo-dT bead and further converted to cDNA and Illumina sequencing library using PrepX RNA-seq library kit on the automated Apollo 324 NGS Library Prep System (Wafergen Biosystems) following the manufacturer's protocol.

Quantification and Statistical Analysis

Analyses on RNA-Seq and modENCODE data were performed on the high-performance computing cluster (64-bit Springdale Linux) at the Lewis-Sigler Institute for Integrative Genomics, Princeton University, using the appropriate packages within the conda environment and package management system. All statistical analyses were performed using R (3.4), Bioconductor packages (3.8), and the conda package management system (4.5.11). Additionally, we utilized custom Unix, Perl, Awk and Sed scripts as necessary. See Supplementary Materials and Methods for greater detail on these analyses.

Acknowledgments

We are grateful to Gary Laevsky and the Molecular Biology Confocal Imaging Facility; Wei Wang, Lance Parsons, Robert Leach, and the Lewis-Sigler Institute Genomics Core Facility; Gordon Gray and the *Drosophila* Media Core Facility at Princeton University; and Michael Denieu and Christopher H. Chandler for technical support. We thank Nareg Djabrayan, Eric Wieschaus, Martin Wühr, Stas Shvartsman, and Jan Skotheim for discussion and critical reading of the manuscript. We are grateful to Shelby Blythe for helpful discussion and technical assistance. Stocks obtained from the Bloomington *Drosophila* Stock Center (NIH P40OD018537) were used in this study.

Competing Interests

The authors declare no competing or financial interests.

Funding

Research funding provided by the Lewis-Sigler Fellows program at Princeton University.

Data Availability

All raw and processed data will be uploaded to NCBI GEO and the link will be made available at the time of publication.

References:

Adamson, E. D. and Woodland, H. R. (1974). Histone synthesis in early amphibian development: Histone and DNA syntheses are not co-ordinated. *Journal of Molecular Biology* **88**, 263–285.

Almouzni, G. and Wolffe, A. P. (1995). Constraints on transcriptional activator function contribute to transcriptional quiescence during early Xenopus embryogenesis. *EMBO J.* **14**, 1752–1765.

Almouzni, G., Méchali, M. and Wolffe, A. P. (1990). Competition between transcription complex assembly and chromatin assembly on replicating DNA. *EMBO J.* **9**, 573–582.

Almouzni, G., Méchali, M. and Wolffe, A. P. (1991). Transcription complex disruption caused by a transition in chromatin structure. *Molecular and Cellular Biology* **11**, 655–665.

Amodeo, A. A., Jukam, D., Straight, A. F. and Skotheim, J. M. (2015). Histone titration against the genome sets the DNA-to-cytoplasm threshold for the *Xenopus* midblastula transition. *Proceedings of the National Academy of Sciences* **112**, E1086–E1095.

Aronesty, E. (2013). Comparison of Sequencing Utility Programs. *The Open Bioinformatics Journal* **7**, 1–8.

Berloco, M., Fanti, L., Breiling, A., Orlando, V. and Pimpinelli, S. (2001). The maternal effect gene, abnormal oocyte (abo), of Drosophila melanogaster encodes a specific negative regulator of histones. *Proceedings of the National Academy of Sciences* **98**, 12126–12131.

Blythe, S. A. and Wieschaus, E. F. (2015a). Coordinating Cell Cycle Remodeling with Transcriptional Activation at the Drosophila MBT. In *Current Topics in Developmental Biology*, pp. 113–148. Elsevier.

Blythe, S. A. and Wieschaus, E. F. (2015b). Zygotic Genome Activation Triggers the DNA Replication Checkpoint at the Midblastula Transition. *Cell* **160**, 1169–1181.

Blythe, S. A. and Wieschaus, E. F. (2016). Establishment and maintenance of heritable chromatin structure during early Drosophila embryogenesis. *eLife* **5**,.

Chen, K., Johnston, J., Shao, W., Meier, S., Staber, C. and Zeitlinger, J. (2013). A global change in RNA polymerase II pausing during the Drosophila midblastula transition. *eLife* **2**,.

Collart, C., Allen, G. E., Bradshaw, C. R., Smith, J. C. and Zegerman, P. (2013). Titration of Four Replication Factors Is Essential for the Xenopus laevis Midblastula Transition. *Science* **341**, 893–896.

David, G., Grandinetti, K. B., Finnerty, P. M., Simpson, N., Chu, G. C. and DePinho, R. A. (2008). Specific requirement of the chromatin modifier mSin3B in cell cycle exit and cellular differentiation. *Proceedings of the National Academy of Sciences* **105**, 4168–4172.

De Renzis, S., Elemento, O., Tavazoie, S. and Wieschaus, E. F. (2007). Unmasking activation of the zygotic genome using chromosomal deletions in the Drosophila embryo. *PLoS Biol.* **5**, e117.

Deneke, V. E., Melbinger, A., Vergassola, M. and Di Talia, S. (2016). Waves of Cdk1 Activity in S Phase Synchronize the Cell Cycle in Drosophila Embryos. *Dev. Cell* **38**, 399–412.

Di Talia, S., She, R., Blythe, S. A., Lu, X., Zhang, Q. F. and Wieschaus, E. F. (2013). Posttranslational Control of Cdc25 Degradation Terminates Drosophila's Early Cell-Cycle Program. *Current Biology* **23**, 127–132.

Djabrayan, N. J.-V., Smits, C. M., Krajnc, M., Stern, T., Yamada, S., Lemon, W. C., Keller, P. J., Rushlow, C. A. and Shvartsman, S. Y. (2019). Metabolic Regulation of Developmental Cell Cycles and Zygotic Transcription. *Current Biology* **29**, 1193-1198.e5.

Dominski, Z., Yang, X. -c., Raska, C. S., Santiago, C., Borchers, C. H., Duronio, R. J. and Marzluff, W. F. (2002). 3' End Processing of Drosophilamelanogaster Histone Pre-mRNAs: Requirement for Phosphorylated Drosophila Stem-Loop Binding Protein and Coevolution of the Histone Pre-mRNA Processing System. *Molecular and Cellular Biology* **22**, 6648–6660.

Driever, W. and Nüsslein-Volhard, C. (1989). The bicoid protein is a positive regulator of hunchback transcription in the early Drosophila embryo. *Nature* **337**, 138–143.

Farrell, J. A. and O'Farrell, P. H. (2013). Mechanism and Regulation of Cdc25/Twine Protein Destruction in Embryonic Cell-Cycle Remodeling. *Current Biology* **23**, 118–126.

Farrell, J. A. and O'Farrell, P. H. (2014). From Egg to Gastrula: How the Cell Cycle Is Remodeled During the *Drosophila* Mid-Blastula Transition. *Annual Review of Genetics* **48**, 269–294.

Fasulo, B., Koyama, C., Yu, K. R., Homola, E. M., Hsieh, T. S., Campbell, S. D. and Sullivan, W. (2012). Chk1 and Wee1 kinases coordinate DNA replication, chromosome condensation, and anaphase entry. *Molecular Biology of the Cell* **23**, 1047–1057.

Foe, V. E. and Alberts, B. M. (1983). Studies of nuclear and cytoplasmic behaviour during the five mitotic cycles that precede gastrulation in Drosophila embryogenesis. *J. Cell. Sci.* **61**, 31–70.

Fogarty, P., Kalpin, R. F. and Sullivan, W. (1994). The Drosophila maternal-effect mutation grapes causes a metaphase arrest at nuclear cycle 13. *Development* **120**, 2131–2142.

Fogarty, P., Campbell, S. D., Abu-Shumays, R., Phalle, B. de S., Yu, K. R., Uy, G. L., Goldberg, M. L. and Sullivan, W. (1997). The Drosophila grapes gene is related to checkpoint gene chk1/rad27 and is required for late syncytial division fidelity. *Current Biology* **7**, 418–426.

Gaertner, B., Johnston, J., Chen, K., Wallaschek, N., Paulson, A., Garruss, A. S., Gaudenz, K., De Kumar, B., Krumlauf, R. and Zeitlinger, J. (2012). Poised RNA Polymerase II Changes over Developmental Time and Prepares Genes for Future Expression. *Cell Reports* **2**, 1670–1683.

Grosshans, J., Müller, H. A. J. and Wieschaus, E. (2003). Control of cleavage cycles in Drosophila embryos by frühstart. *Dev. Cell* **5**, 285–294.

Groth, A., Corpet, A., Cook, A. J. L., Roche, D., Bartek, J., Lukas, J. and Almouzni, G. (2007). Regulation of Replication Fork Progression Through Histone Supply and Demand. *Science* **318**, 1928–1931.

Günesdogan, U., Jäckle, H. and Herzig, A. (2010). A genetic system to assess in vivo the functions of histones and histone modifications in higher eukaryotes. *EMBO Rep.* **11**, 772–776.

Günesdogan, U., Jäckle, H. and Herzig, A. (2014). Histone supply regulates S phase timing and cell cycle progression. *eLife* **3**,.

Gunjan, A. and Verreault, A. (2003). A Rad53 kinase-dependent surveillance mechanism that regulates histone protein levels in S. cerevisiae. *Cell* **115**, 537–549.

Harrison, M. M. and Eisen, M. B. (2015). Transcriptional Activation of the Zygotic Genome in Drosophila. In *Current Topics in Developmental Biology*, pp. 85–112. Elsevier.

Harrison, M. M., Botchan, M. R. and Cline, T. W. (2010). Grainyhead and Zelda compete for binding to the promoters of the earliest-expressed Drosophila genes. *Developmental Biology* **345**, 248–255.

Harrison, M. M., Li, X.-Y., Kaplan, T., Botchan, M. R. and Eisen, M. B. (2011). Zelda Binding in the Early Drosophila melanogaster Embryo Marks Regions Subsequently Activated at the Maternal-to-Zygotic Transition. *PLoS Genetics* **7**, e1002266.

He, W.-X., Wu, M., Liu, Z., Li, Z., Wang, Y., Zhou, J., Yu, P., Zhang, X.-J., Zhou, L. and Gui, J.-F. (2018). Oocyte-specific maternal Slbp2 is required for replication-dependent histone storage and early nuclear cleavage in zebrafish oogenesis and embryogenesis. *RNA* **24**, 1738–1748.

Horard, B. and Loppin, B. (2015). Histone storage and deposition in the early Drosophila embryo. *Chromosoma* **124**, 163–175.
Huber, W., Carey, V. J., Gentleman, R., Anders, S., Carlson, M., Carvalho, B. S., Bravo, H. C., Davis, S., Gatto, L., Girke, T., et al. (2015). Orchestrating high-throughput genomic analysis with Bioconductor. *Nature Methods* **12**, 115–121.
Hug, C. B., Grimaldi, A. G., Kruse, K. and Vaquerizas, J. M. (2017). Chromatin Architecture Emerges during Zygotic Genome Activation Independent of Transcription. *Cell* **169**, 216-228.e19.
Iampietro, C., Bergalet, J., Wang, X., Cody, N. A. L., Chin, A., Lefebvre, F. A., Douziech, M., Krause, H. M. and Lécuyer, E. (2014). Developmentally Regulated Elimination of Damaged Nuclei Involves a Chk2-Dependent Mechanism of mRNA Nuclear Retention. *Developmental Cell* **29**, 468–481.
Ji, J.-Y., Squirrell, J. M. and Schubiger, G. (2004). Both cyclin B levels and DNA-replication checkpoint control the early embryonic mitoses in Drosophila. *Development* **131**, 401–411.
Joseph, S. R., Pálfy, M., Hilbert, L., Kumar, M., Karschau, J., Zaburdaev, V., Shevchenko, A. and Vastenhouw, N. L. (2017). Competition between histone and transcription factor binding regulates the onset of transcription in zebrafish embryos. *eLife* **6**,.
Kadosh, D. and Struhl, K. (1998). Histone deacetylase activity of Rpd3 is important for transcriptional repression in vivo. *Genes Dev.* **12**, 797–805.
Lanzotti, D. J., Kaygun, H., Yang, X., Duronio, R. J. and Marzluff, W. F. (2002). Developmental Control of Histone mRNA and dSLBP Synthesis during Drosophila Embryogenesis and the Role of dSLBP in Histone mRNA 3’ End Processing In Vivo. *Molecular and Cellular Biology* **22**, 2267–2282.
Lee, M. T., Bonneau, A. R., Takacs, C. M., Bazzini, A. A., DiVito, K. R., Fleming, E. S. and Giraldez, A. J. (2013). Nanog, Pou5f1 and SoxB1 activate zygotic gene expression during the maternal-to-zygotic transition. *Nature* **503**, 360–364.
Lefebvre, F. A., Benoit Bouvrette, L. P., Bergalet, J. and Lécuyer, E. (2017). Biochemical Fractionation of Time-Resolved Drosophila Embryos Reveals Similar Transcriptomic Alterations in Replication Checkpoint and Histone mRNA Processing Mutants. *J. Mol. Biol.* **429**, 3264–3279.
Leichsenring, M., Maes, J., Mossner, R., Driever, W. and Onichtchouk, D. (2013). Pou5f1 Transcription Factor Controls Zygotic Gene Activation In Vertebrates. *Science* **341**, 1005–1009.
Li, X.-Y., Harrison, M. M., Villalta, J. E., Kaplan, T. and Eisen, M. B. (2014). Establishment of regions of genomic activity during the Drosophila maternal to zygotic transition. *Elife* **3**,.
Liang, H.-L., Nien, C.-Y., Liu, H.-Y., Metzstein, M. M., Kirov, N. and Rushlow, C. (2008). The zinc-finger protein Zelda is a key activator of the early zygotic genome in Drosophila. *Nature* **456**, 400–403.
Liu, B., Winkler, F., Herde, M., Witte, C.-P. and Großhans, J. (2019). A Link between Deoxyribonucleotide Metabolites and Embryonic Cell-Cycle Control. *Current Biology* **29**, 1187-1192.e3.
Lott, S. E., Villalta, J. E., Schroth, G. P., Luo, S., Tonkin, L. A. and Eisen, M. B. (2011). Noncanonical Compensation of Zygotic X Transcription in Early Drosophila melanogaster Development Revealed through Single-Embryo RNA-Seq. *PLoS Biology* **9**, e1000590.
Love, M. I., Huber, W. and Anders, S. (2014). Moderated estimation of fold change and dispersion for RNA-seq data with DESeq2. *Genome Biology* **15**,.
Lu, X., Li, J. M., Elemento, O., Tavazoie, S. and Wieschaus, E. F. (2009). Coupling of zygotic transcription to mitotic control at the Drosophila mid-blastula transition. *Development* **136**, 2101–2110.

modENCODE Consortium, Celniker, S. E., Dillon, L. A. L., Gerstein, M. B., Gunsalus, K. C., Henikoff, S., Karpen, G. H., Kellis, M., Lai, E. C., Lieb, J. D., et al. (2009). Unlocking the secrets of the genome. *Nature* **459**, 927–930.

Newport, J. and Kirschner, M. (1982a). A major developmental transition in early xenopus embryos: I. characterization and timing of cellular changes at the midblastula stage. *Cell* **30**, 675–686.

Newport, J. and Kirschner, M. (1982b). A major developmental transition in early xenopus embryos: II. control of the onset of transcription. *Cell* **30**, 687–696.

O'Connell, M. J., Raleigh, J. M., Verkade, H. M. and Nurse, P. (1997). Chk1 is a wee1 kinase in the G2 DNA damage checkpoint inhibiting cdc2 by Y15 phosphorylation. *EMBO J.* **16**, 545–554.

Patro, R., Duggal, G., Love, M. I., Irizarry, R. A. and Kingsford, C. (2017). Salmon provides fast and bias-aware quantification of transcript expression. *Nature Methods* **14**, 417–419.

Peng, A., Lewellyn, A. L. and Maller, J. L. (2007). Undamaged DNA Transmits and Enhances DNA Damage Checkpoint Signals in Early Embryos. *Molecular and Cellular Biology* **27**, 6852–6862.

Pérez-Montero, S., Carbonell, A., Morán, T., Vaquero, A. and Azorín, F. (2013). The Embryonic Linker Histone H1 Variant of Drosophila, dBigH1, Regulates Zygotic Genome Activation. *Developmental Cell* **26**, 578–590.

Perkins, L. A., Holderbaum, L., Tao, R., Hu, Y., Sopko, R., McCall, K., Yang-Zhou, D., Flockhart, I., Binari, R., Shim, H.-S., et al. (2015). The Transgenic RNAi Project at Harvard Medical School: Resources and Validation. *Genetics* **201**, 843–852.

Picelli, S., Faridani, O. R., Björklund, Å. K., Winberg, G., Sagasser, S. and Sandberg, R. (2014). Full-length RNA-seq from single cells using Smart-seq2. *Nature Protocols* **9**, 171–181.

Pile, L. A., Schlag, E. M. and Wassarman, D. A. (2002). The SIN3/RPD3 Deacetylase Complex Is Essential for G2 Phase Cell Cycle Progression and Regulation of SMRTER Corepressor Levels. *Molecular and Cellular Biology* **22**, 4965–4976.

Prado, F. and Aguilera, A. (2005). Partial Depletion of Histone H4 Increases Homologous Recombination-Mediated Genetic Instability. *Molecular and Cellular Biology* **25**, 1526–1536.

Price, D., Rabinovitch, S., O'Farrell, P. H. and Campbell, S. D. (2000). Drosophila wee1 has an essential role in the nuclear divisions of early embryogenesis. *Genetics* **155**, 159–166.

Prioleau, M. N., Huet, J., Sentenac, A. and Méchali, M. (1994). Competition between chromatin and transcription complex assembly regulates gene expression during early development. *Cell* **77**, 439–449.

Rau, A., Marot, G. and Jaffrézic, F. (2014). Differential meta-analysis of RNA-seq data from multiple studies. *BMC Bioinformatics* **15**, 91.

Royou, A., McCusker, D., Kellogg, D. R. and Sullivan, W. (2008). Grapes(Chk1) prevents nuclear CDK1 activation by delaying cyclin B nuclear accumulation. *The Journal of Cell Biology* **183**, 63–75.

Schindelin, J., Arganda-Carreras, I., Frise, E., Kaynig, V., Longair, M., Pietzsch, T., Preibisch, S., Rueden, C., Saalfeld, S., Schmid, B., et al. (2012). Fiji: an open-source platform for biological-image analysis. *Nature Methods* **9**, 676–682.

Seller, C. A. and O'Farrell, P. H. (2018). Rif1 prolongs the embryonic S phase at the Drosophila mid-blastula transition. *PLOS Biology* **16**, e2005687.

Shermoen, A. W., McCleland, M. L. and O'Farrell, P. H. (2010). Developmental Control of Late Replication and S Phase Length. *Current Biology* **20**, 2067–2077.

Shimuta, K., Nakajo, N., Uto, K., Hayano, Y., Okazaki, K. and Sagata, N. (2002). Chk1 is activated transiently and targets Cdc25A for degradation at the Xenopus midblastula transition. *EMBO J.* **21**, 3694–3703.

Shindo, Y. and Amodeo, A. A. (2019). Dynamics of Free and Chromatin-Bound Histone H3 during Early Embryogenesis. *Current Biology*.

Sibon, O. C., Stevenson, V. A. and Theurkauf, W. E. (1997). DNA-replication checkpoint control at the Drosophila midblastula transition. *Nature* **388**, 93–97.
Sibon, O. C. M., Laurençon, A., Scott Hawley, R. and Theurkauf, W. E. (1999). The Drosophila ATM homologue Mei-41 has an essential checkpoint function at the midblastula transition. *Current Biology* **9**, 302–312.
Silverstein, R. A. and Ekwall, K. (2005). Sin3: a flexible regulator of global gene expression and genome stability. *Current Genetics* **47**, 1–17.
Song, Y., Marmion, R. A., Park, J. O., Biswas, D., Rabinowitz, J. D. and Shvartsman, S. Y. (2017). Dynamic Control of dNTP Synthesis in Early Embryos. *Developmental Cell* **42**, 301-308.e3.
Stumpff, J., Duncan, T., Homola, E., Campbell, S. D. and Su, T. T. (2004). Drosophila Wee1 Kinase Regulates Cdk1 and Mitotic Entry during Embryogenesis. *Current Biology* **14**, 2143–2148.
Sullivan, E., Santiago, C., Parker, E. D., Dominski, Z., Yang, X., Lanzotti, D. J., Ingledue, T. C., Marzluff, W. F. and Duronio, R. J. (2001). Drosophila stem loop binding protein coordinates accumulation of mature histone mRNA with cell cycle progression. *Genes Dev.* **15**, 173–187.
Sung, H., Spangenberg, S., Vogt, N. and Großhans, J. (2013). Number of Nuclear Divisions in the Drosophila Blastoderm Controlled by Onset of Zygotic Transcription. *Current Biology* **23**, 133–138.
Tadros, W. and Lipshitz, H. D. (2009). The maternal-to-zygotic transition: a play in two acts. *Development* **136**, 3033–3042.
Tomkiel, J., Pimpinelli, S. and Sandler, L. (1991). Rescue from the abnormal oocyte maternal-effect lethality by ABO heterochromatin in Drosophila melanogaster. *Genetics* **128**, 583–594.
Tomkiel, J., Fanti, L., Berloco, M., Spinelli, L., Tamkun, J. W., Wakimoto, B. T. and Pimpinelli, S. (1995). Developmental genetical analysis and molecular cloning of the abnormal oocyte gene of Drosophila melanogaster. *Genetics* **140**, 615–627.
Vastag, L., Jorgensen, P., Peshkin, L., Wei, R., Rabinowitz, J. D. and Kirschner, M. W. (2011). Remodeling of the Metabolome during Early Frog Development. *PLoS ONE* **6**, e16881.
Vastenhouw, N. L., Cao, W. X. and Lipshitz, H. D. (2019). The maternal-to-zygotic transition revisited. *Development* **146**, dev161471.
Woodland, H. R. and Adamson, E. D. (1977). The synthesis and storage of histones during the oogenesis of Xenopus laevis. *Developmental Biology* **57**, 118–135.
Ye, X., Franco, A. A., Santos, H., Nelson, D. M., Kaufman, P. D. and Adams, P. D. (2003). Defective S phase chromatin assembly causes DNA damage, activation of the S phase checkpoint, and S phase arrest. *Mol. Cell* **11**, 341–351.
Yu, G., Wang, L.-G. and He, Q.-Y. (2015). ChIPseeker: an R/Bioconductor package for ChIP peak annotation, comparison and visualization. *Bioinformatics* **31**, 2382–2383.
Yuan, K., Seller, C. A., Shermoen, A. W. and O'Farrell, P. H. (2016). Timing the Drosophila Mid-Blastula Transition: A Cell Cycle-Centered View. *Trends in Genetics* **32**, 496–507.
Zhang, W., Zhang, X., Xue, Z., Li, Y., Ma, Q., Ren, X., Zhang, J., Yang, S., Yang, L., Wu, M., et al. (2018). Probing the Function of Metazoan Histones with a Systematic Library of H3 and H4 Mutants. *Developmental Cell*.
Zhu, A., Ibrahim, J. G. and Love, M. I. (2018). Heavy-tailed prior distributions for sequence count data: removing the noise and preserving large differences. *Bioinformatics*.

Figures

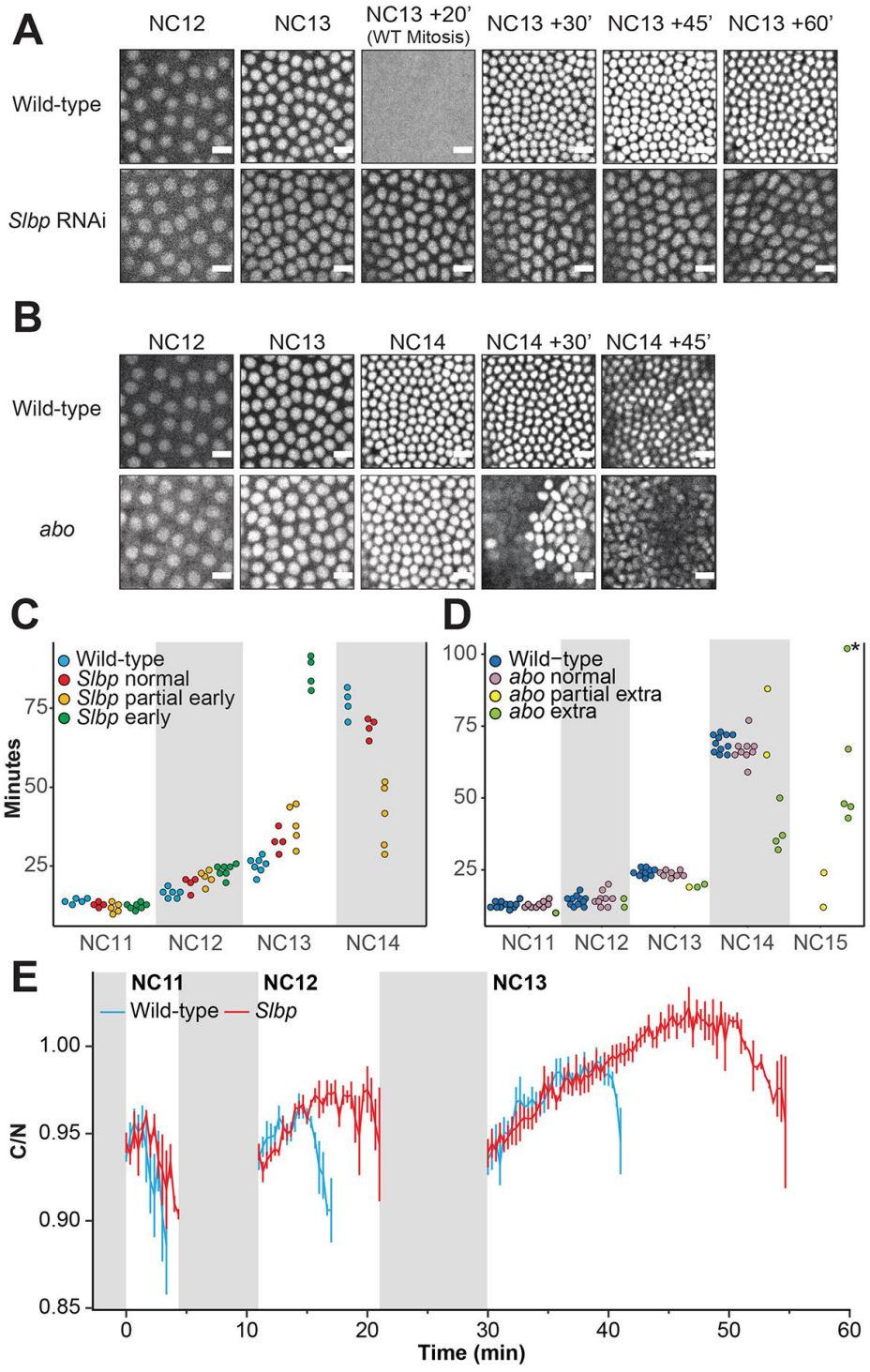

Figure 1. Changes to replication-dependent histone concentration alter cell cycle and timing at the MBT.

(A-B) Still frames from time-lapse imaging of wild-type (WT), *Slbp* (histone knockdown), and *abo* (histone overexpression) embryos from NC12 through gastrulation. Nuclei were visualized using an nls-RFP marker. ~50% of *Slbp* embryos that form a blastoderm do not undergo a 13th mitosis (shown). WT embryos mitose into NC14, ~20 minutes after entering NC13, but these *Slbp* embryos remain in

NC13 where they cellularize, then gastrulate at lower nuclear densities. ~30% of *Slbp* embryos that form a blastoderm undergo a partial 13th mitosis. Conversely, ~6% of observed *abo* embryos have a shortened NC14 before undergoing a full extra mitosis and attempting a catastrophic gastrulation at NC15 while another ~4% undergo a partial extra mitosis (shown). Scale bar represents 10 μm. (C) Scatterplot of *Slbp* cell cycle times compared to WT. Cell cycle times were predictive of phenotype with longer early cycles in *Slbp* associated with full arrest in NC13. (D) Scatterplot for *abo* cell cycle times compared to WT. Shorter early cycles in *abo* are associated with extra divisions. NC15 data point with asterisk (*) denotes an embryo underwent a 16th nuclear cycle. (E) Cytoplasmic to nuclear ratio (C/N) of the Chk1 biosensor in wild-type (blue, n=4) and *Slbp* (red, n=4) embryo from NC11-NC13. Chk1 is prematurely activated in *Slbp* embryos that have lengthened early cell cycles but do not undergo premature gastrulation. Grey boxes represent mitosis. Bars represent mean and SEM.

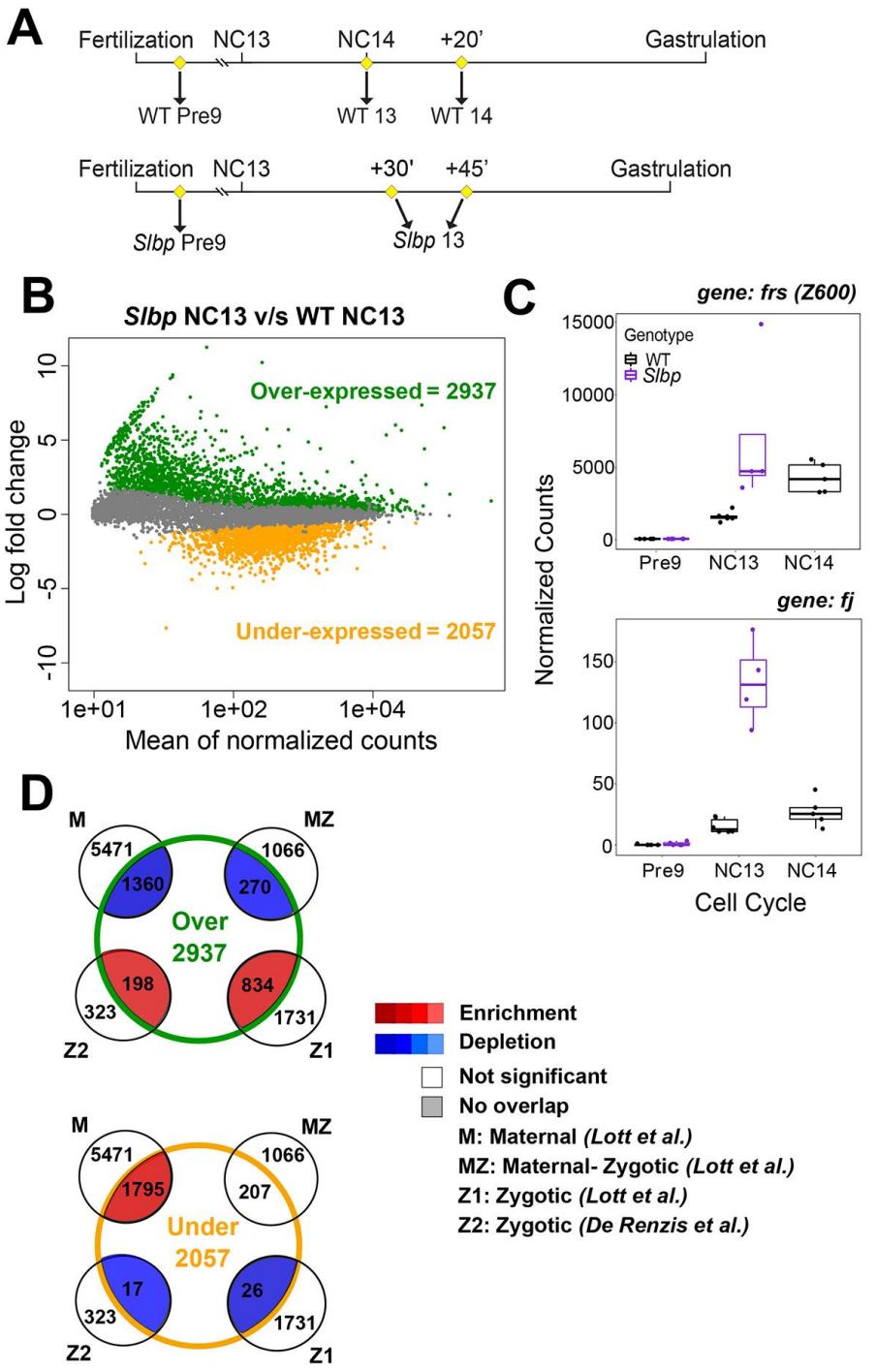

Figure 2. Depletion of maternal histones results in an early ZGA.
(A) Schematic of embryo collection for *Slbp* RNA-seq. Pre-NC9 embryos were collected for both WT (n=5) and *Slbp* (n=5) to control for maternal loading. *Slbp* embryos were collected 30 or 45 minutes into NC13 (n=4) to ensure embryo health and phenotype and compared to nuclear cycle matched (mitosis of NC13) (n=6) or time matched (20 minutes into NC14) (n=5) WT embryos. (B) When compared to WT NC13, 2937 genes are overexpressed and 2057 genes are underexpressed in *Slbp* embryos. (C) Traces from two overexpressed genes, *frs* and *fj*. (D) Data from B compared to previous datasets. When compared to nuclear cycle matched controls,

overexpressed transcripts are enriched for genes zygotically expressed genes and de-enriched maternal transcripts. Conversely, underexpressed genes are enriched for maternally and de-enriched for new zygotic transcripts. This pattern is consistent with premature ZGA. Comparisons to time matched controls yield similar results (Figure S3).

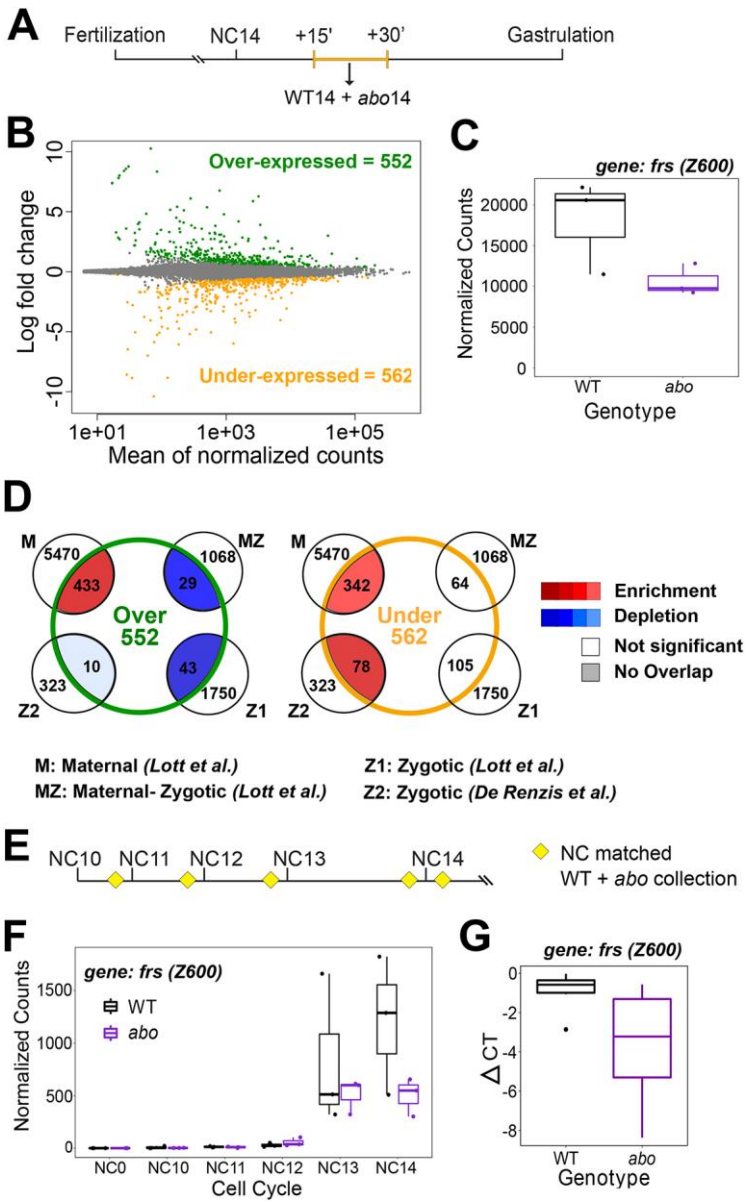

Figure 3. Overexpression of maternal histones delays ZGA.
(A) Schematic of embryo collection for B and C. Pooled *abo* (n=3) or WT (n=3) embryos were collected between 15 and 30 minutes into NC14. (B) 552 genes are overexpressed and 562 genes are underexpressed in *abo* embryos in NC14 compared to WT. (C) A representative trace of a zygotic gene (*frs*) that is differentially expressed in B. (D) Genes that are overexpressed in *abo* are enriched for maternal genes and those that are underexpressed are enriched for both maternal and zygotic genes. (E) Schematic of time course embryo collection. Embryos were collected at the last three minutes of NC10-13 (n=3 per time point) and the first three minutes of NC14 (n=3). (F) A representative trace of a zygotic gene (*frs*) that is differentially expressed in NC 14. (G) Single embryo qPCR of *frs* in NC14 *abo* and WT embryos (Delta CT normalized to RpL32).

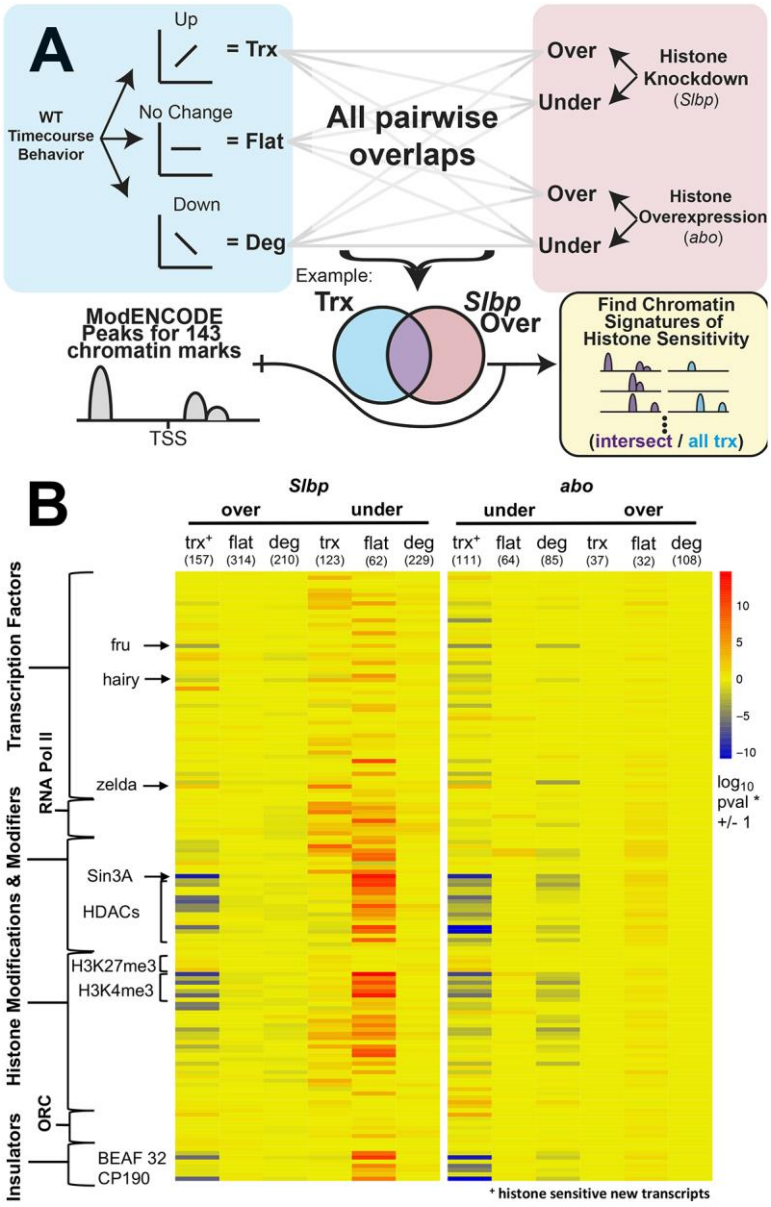

Figure 4. Histone sensitive transcripts share common chromatin features. (A) Schematic of enrichment calculation. Genes were categorized as new transcription (Trx), flat, or maternally degraded (Deg) based on their behavior between NC9 and NC14 in WT embryos (Fig 2A). Next, significantly under and overexpressed genes were identified from time matched datasets for both *Slbp* (*Slbp* NC13 compared to WT NC14; Figure S3D, Table S2 and S17) and *abo* (time course; Figure 3B, Table S2 and S18). These genes were then sorted based on WT behavior as Trx, Flat, or Deg. This yielded 12 pairwise comparisons (e.g., New Transcription & *Slbp* overexpressed, Flat & *Slbp* overexpressed, etc.). Peak occupancy was calculated for all transcriptional start sites +/- 500bp in the genome from 143 modENCODE ChIP-seq and ChIP-chip datasets. Finally, enrichment for peaks from each modENCODE dataset was calculated using Fisher's exact test for each of the above 12 classes over the background class (e.g. the set of newly transcribed genes that were overexpressed in *Slbp* was compared to all newly

transcribed genes). (B) Enrichments for 143 modENCODE datasets for six classes of genes whose expression was changed in *Slbp* or *abo* as described in A. Numbers below each heading denote the number of genes in each category. In both cases histone sensitive new transcripts (the first column of each comparison, marked with a +) were enriched for the pioneer transcription factor, ZLD, and H3K27me3 while de-enriched for class I insulator proteins (BEAF-32 and CP190), H3K4me3, *hairy*, *fruitless*, SIN3A, and its associated histone deacetylases (HDACs).

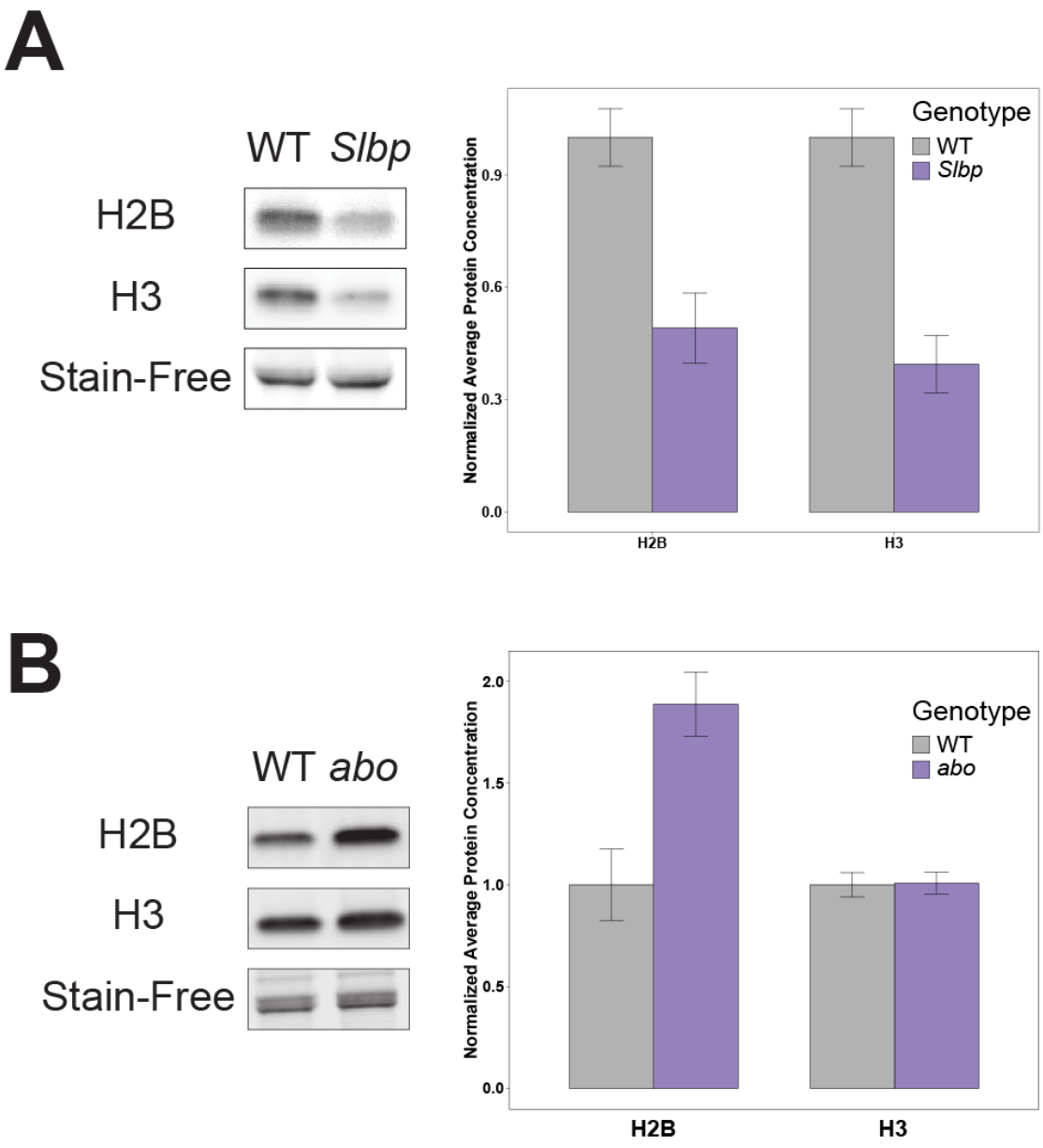

Figure S1. *Slbp* RNAi and *abo* embryos have altered histone protein levels
(A) Total H2B and H3 protein from WT and *Slbp* embryos collected 55 minutes after pole cell formation (early NC14 in WT) from western blotting with 5 embryos per lane. *Slbp* embryos have approximately a ~50% reduction in H2B protein and ~60% reduction in H3 protein (n=3). Bars represent mean and SEM. (B) Total H2B and H3 protein from *abo* embryos at collected 55 minutes after pole cell formation (early NC14 in WT) from western blotting. *abo* embryos have ~90% increase in H2B while total H3 was unchanged between WT (n=5) and *abo* (n=6) embryos. Bars represent mean and SEM. We note that the antibodies used for the assay cannot distinguish between the replication-coupled and replication-independent H3 variants and so the effect size on the replication-coupled H3 may be greater than reported here if there is compensation by the replication-independent variant.

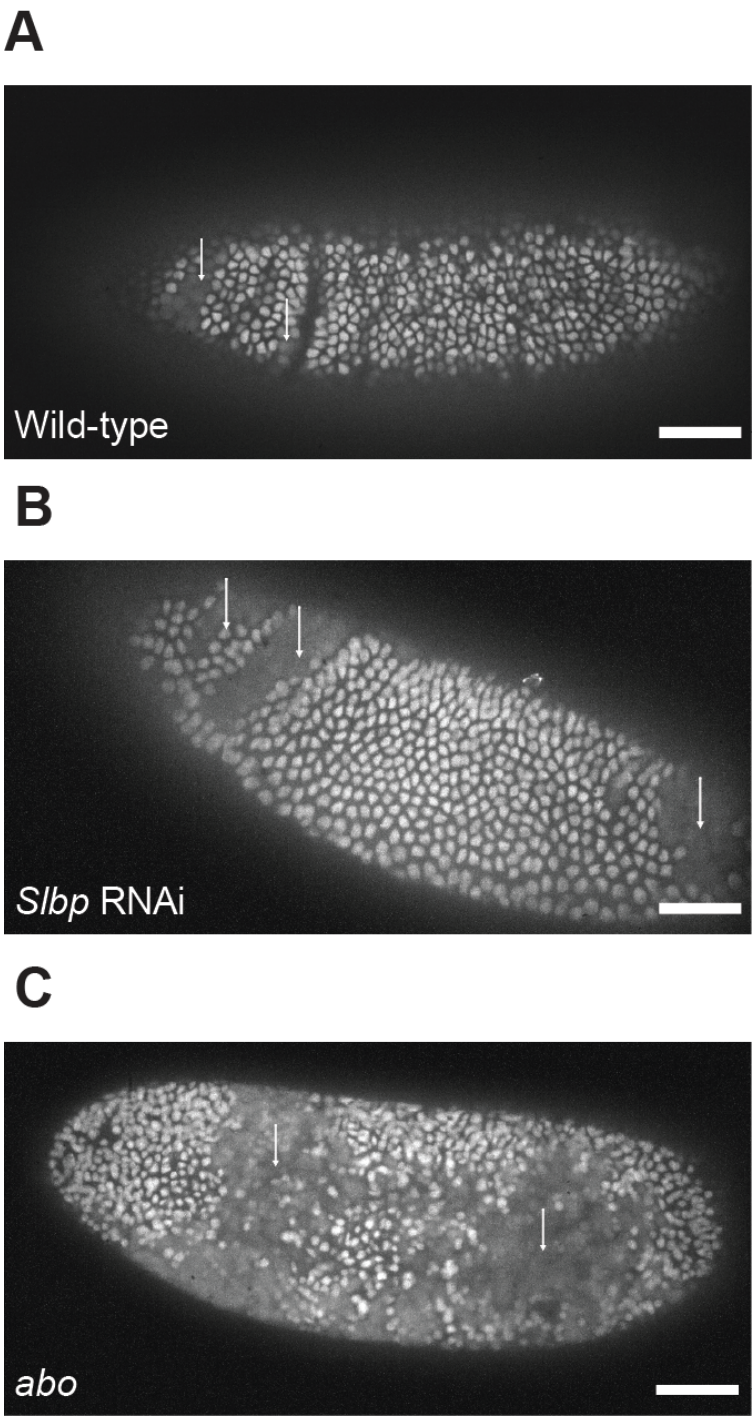

Figure S2. *Slbp* RNAi and *abo* embryos attempt post-MBT development
(A) WT embryo post-MBT after NC14. Mitotic domains and gastrulation movements form normally and with characteristic temporal and spatial dynamics. Arrows indicate mitotic domains. (B) *Slbp* embryo that enters gastrulation in NC13. Mitotic domain formation and gastrulation appear unaffected despite embryos having reduced numbers of cells. These embryos proceed through early-to-mid embryogenesis relatively normally but die before hatching. Arrows indicate mitotic domain formation. (C) *abo* embryos that enters gastrulation in NC15. *abo* embryos that undergo extra divisions still attempt post-MBT behaviors such as mitotic domain formation and gastrulation but are severely disrupted. Arrows indicate aberrant mitotic domain formation. Scale bar represents 50 μm.

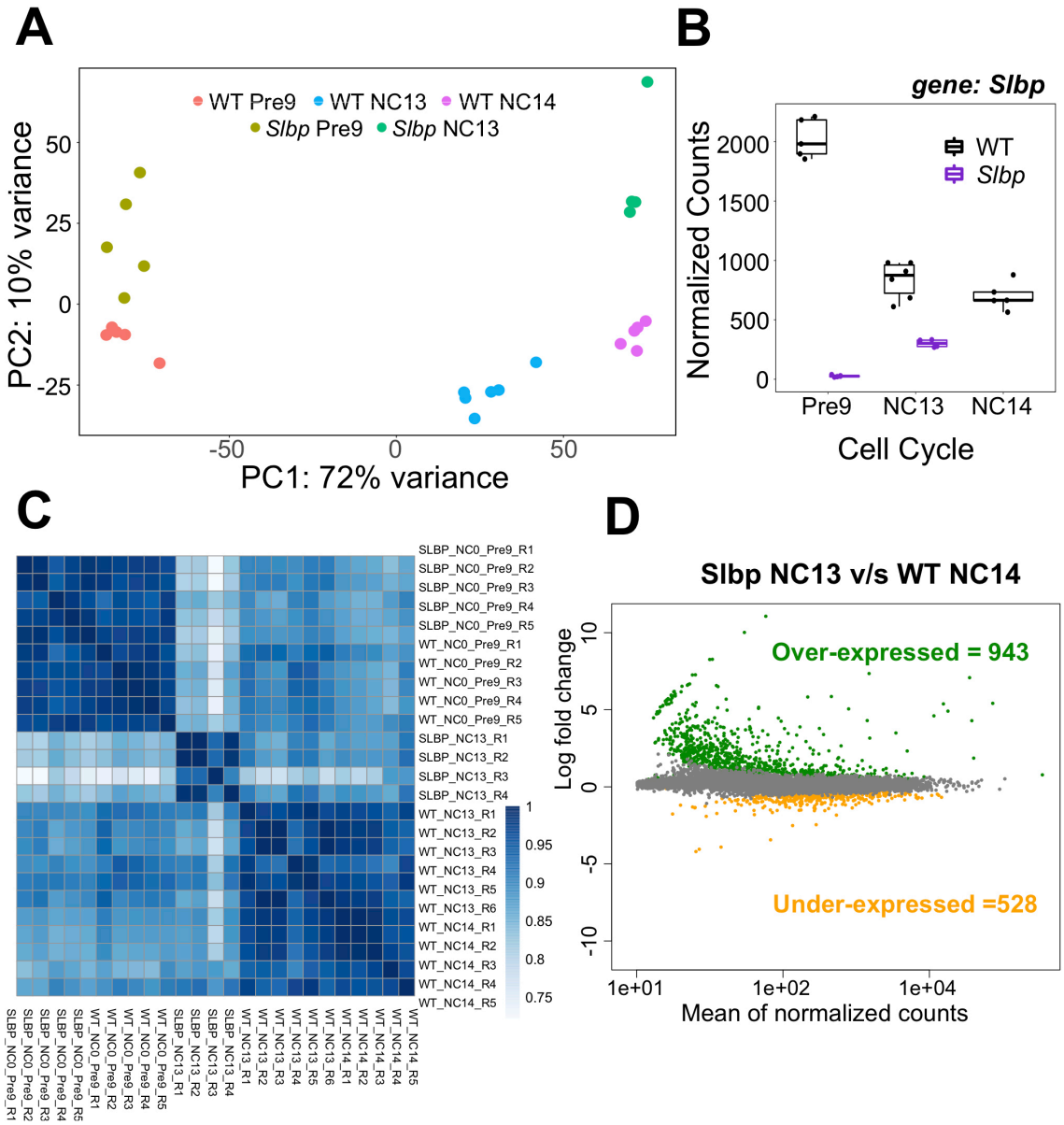

M: Maternal *(Lott et al.)*
MZ: Maternal- Zygotic *(Lott et al.)*
Z1: Zygotic *(Lott et al.)*
Z2: Zygotic *(De Renzis et al.)*

Figure S3. Depletion of maternal histones advance MZT
(A) Principal Components Analysis of *Slbp* and WT expression data demonstrating that global transcriptomic profile is shifted in *Slbp* NC13 as compared WT NC13 and is more similar to WT NC14 indicating that the onset of transcription is advanced in *Slbp* embryos. (B) Normalized counts of *Slbp* mRNA showing a reduction in *Slbp* mutants (n=5 in Pre9 and n=4 in NC13) as compared to WT (n=5 in Pre9, n=6 in NC13 and n=5 in NC14) (C) Spearman's correlation of expression data for WT and *Slbp* embryos at different timepoints. Replicates are more similar to each other than they are to other genotypes and timepoints. (D) When compared to time matched controls (NC14 +20') fewer genes are altered in expression. 943 genes are overexpressed and 528 genes are underexpressed, consistent with premature MZT in the *Slbp* embryos. (E) Data from C compared to previous datasets. Genes overexpressed compared to WT NC14 embryos show enrichment for zygotic transcripts while the underexpressed genes are enriched for maternal transcripts and show a slight enrichment for the De Renzis maternal genes.

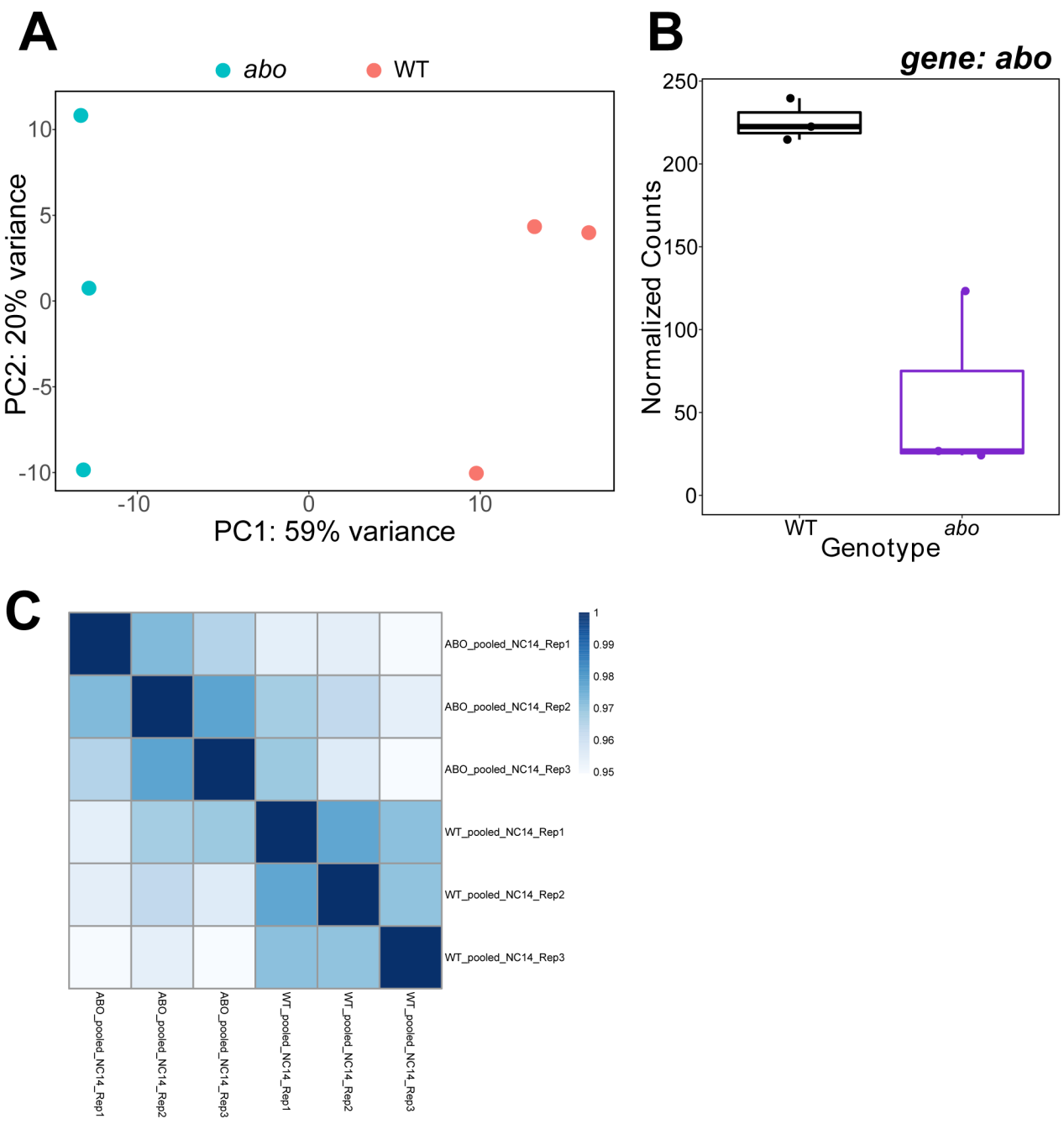

Figure S4. Global transcriptomic differences upon histone overexpression
(A) Principal Components Analysis between the pooled NC14 *abo* and WT expression data showing a clear difference in gene expression between genotypes at this developmental stage. (B) Normalized counts of *abo* mRNA showing reduction in *abo* mutants (n=3) as compared to WT (n=3). (C) Spearman's correlation of expression data for WT and *abo* embryos in NC14.

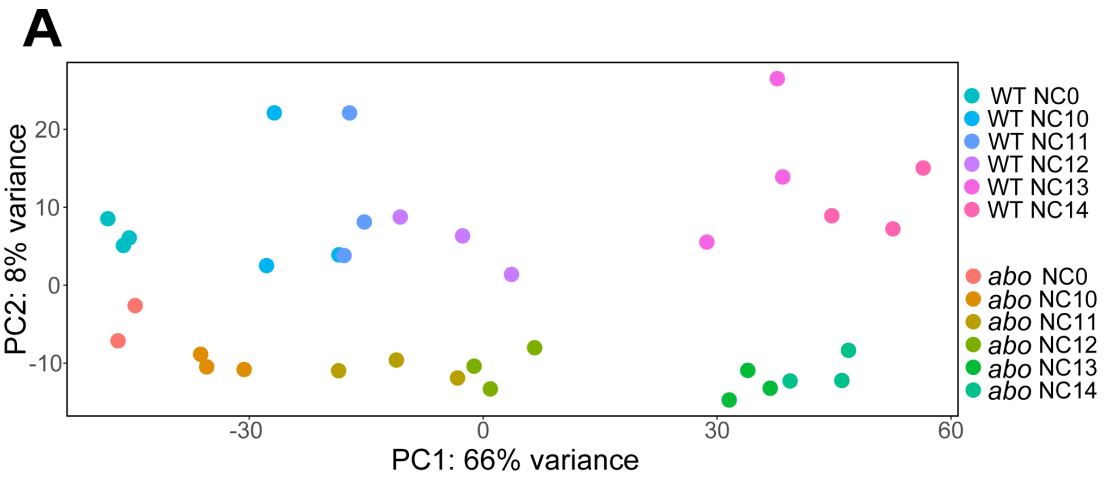

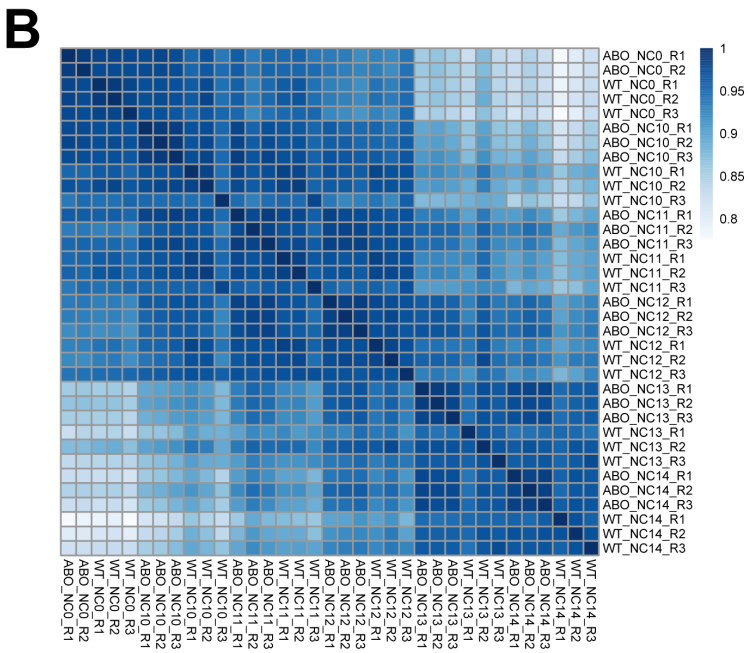

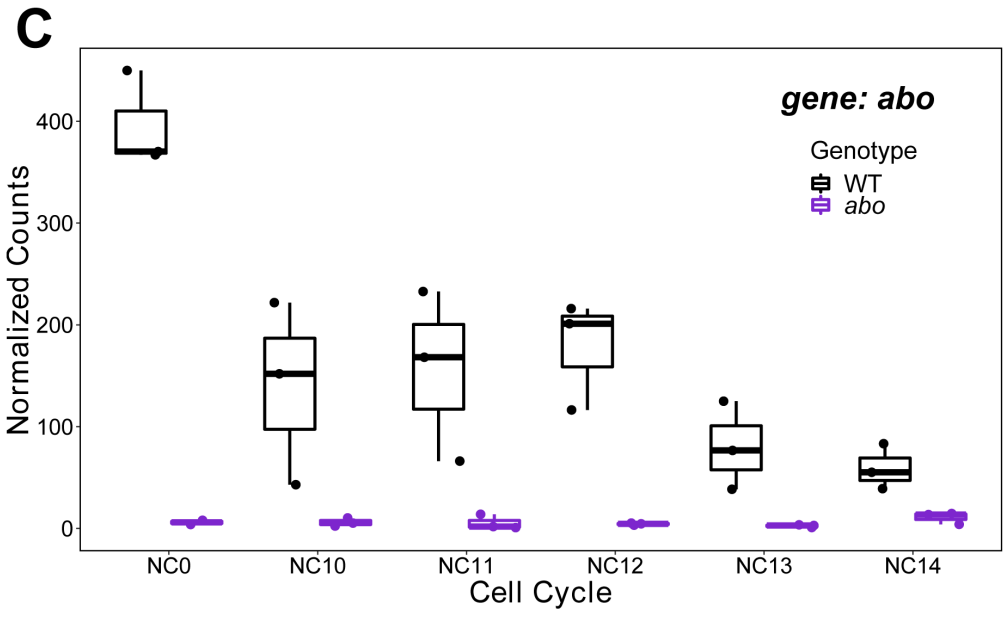

Figure S5. Timecourse transcriptomic differences upon histone overexpression
(A) Principal Components Analysis shows a clear separation across both cell cycle and genotype for the *abo* time-course experiment. (B)Spearman's correlation of expression data for WT and *abo* embryos across all timepoints. (C) Normalized counts of *abo* mRNA showing a reduction in *abo* mutants (n=2 at NC0 and n=3, all other time-points) as compared to WT (n=3, all time-points)

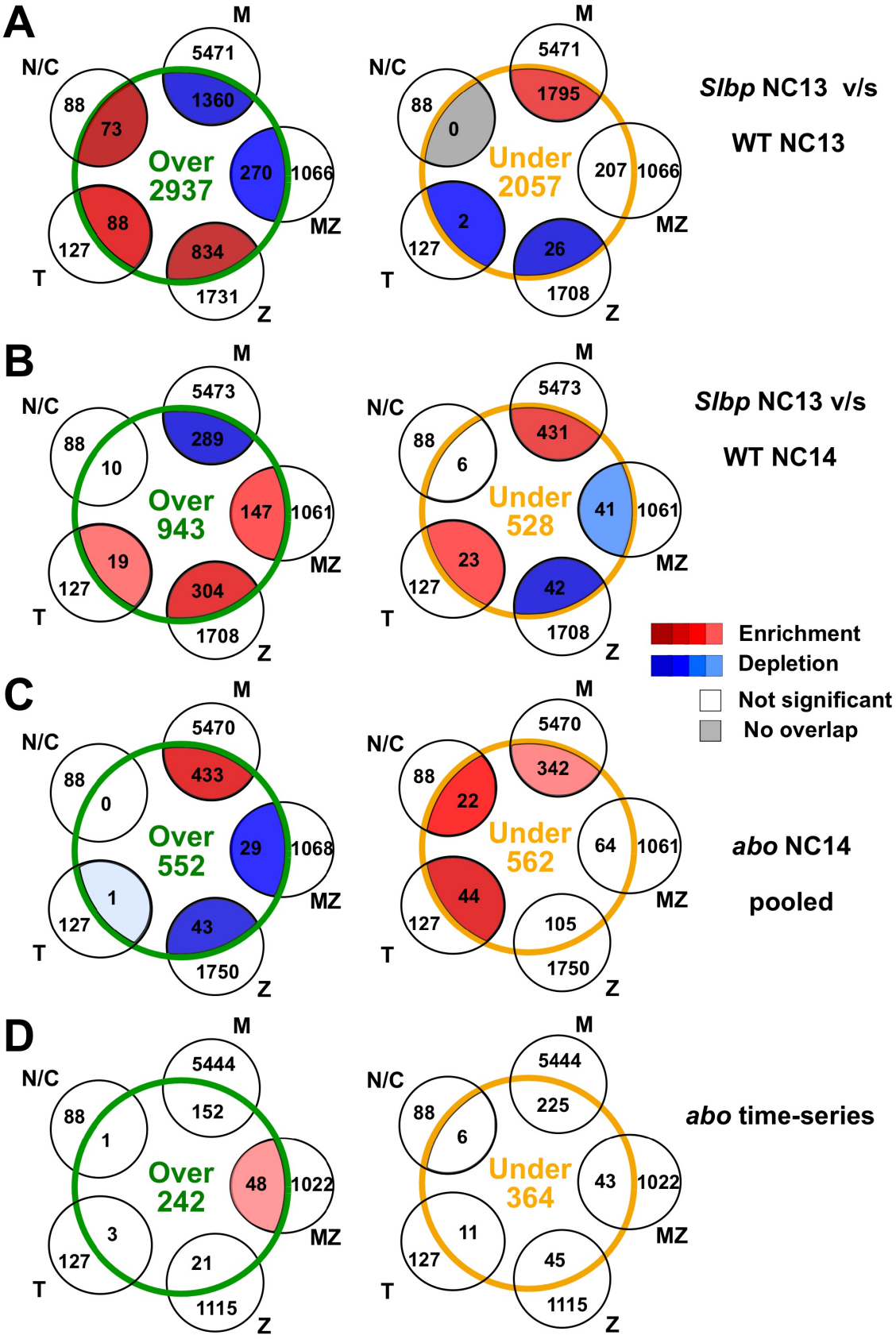

Figure S6. Histone sensitivity changes the onset of ZGA, but cannot explain previous N/C ratio dependent gene sets (A) *Slbp* NC13 compared to WT NC13. Data the same as Figure 2D except the De Renzis et al. (2007) maternal data has been split into N/C and time dependent genes as per Lu et al. (2009). Both N/C and time dependent genes are enriched in the overexpressed and depleted in the underexpressed categories, consistent with global advancement of the MZT. (B) *Slbp* NC13 compared to WT NC14. Data corresponds to Figure S3E. When controlled for time, enrichment of N/C ratio dependent genes is lost and time-dependent genes become enriched in both the over and under expressed gene sets. (C) *abo* NC14 compared to WT NC14. Data corresponds to Figure 3D. Both N/C and time dependent genes are enriched in the underexpressed category consistent with a global delay of ZGA. (D) *abo* time series comparison. Although not statistically significant, both N/C ratio and time dependent genes show an odds ratio >1 indicating these are also trending towards enrichment in the underexpressed gene set. Indeed, when the abo timecourse underexpressed genes are compared to De Renzis et. al (2007) zygotic genes dataset from which the N/C and time gene sets are derived the total zygotic overlap shows significant enrichment (p=9.9e-4) indicating that zygotic genes are better represented in the timecourse abo underexpressed group than the overexpressed set (Table S6).

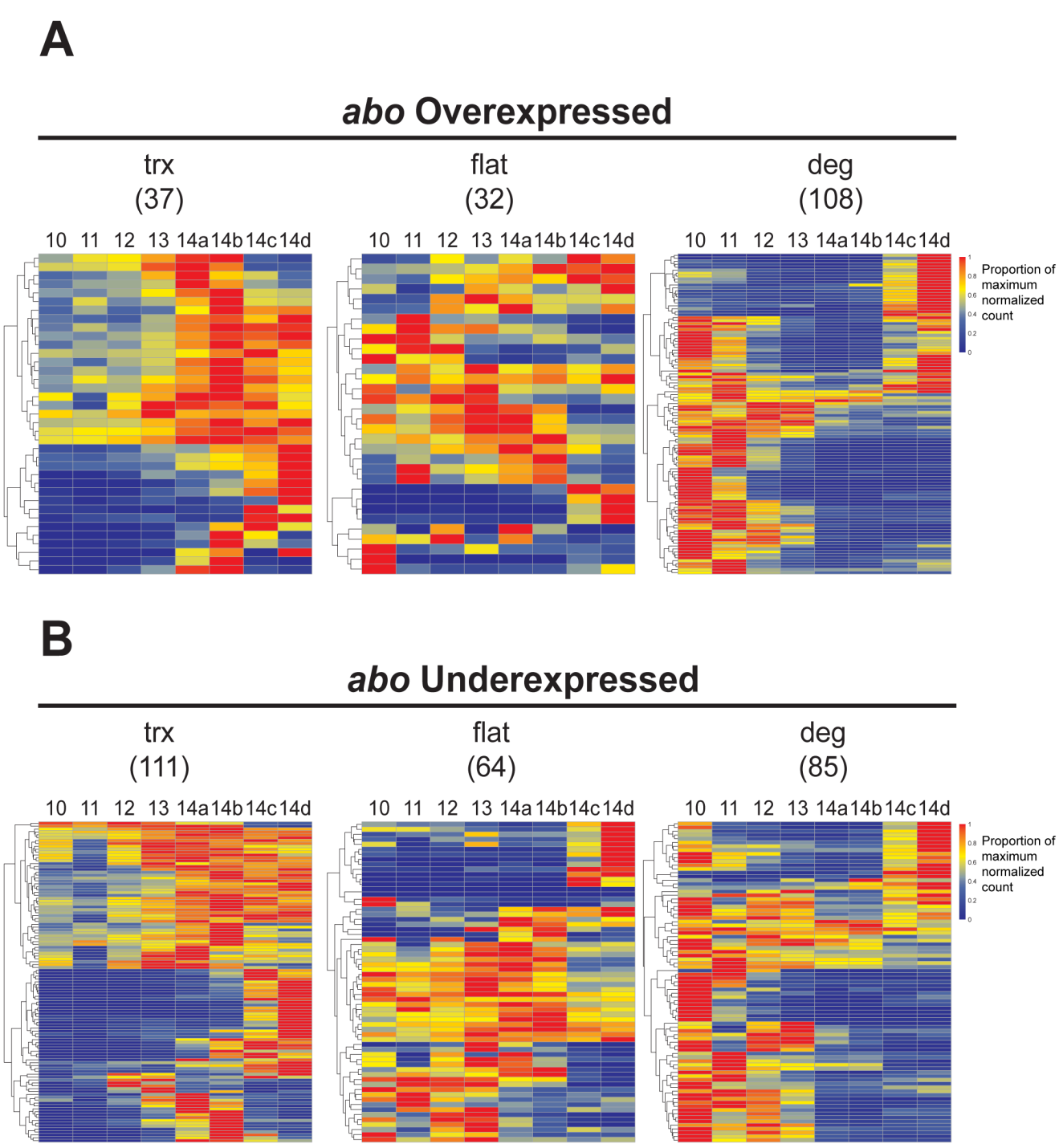

Figure S7. Genes that are knocked down by histone overexpression are expressed during WT MZT

(A) Overexpressed genes in the *abo* time series compared to longer time course from Lott et al. (2011). Each heatmap represents genes categorized as increasing (trx), remaining constant (flat), or decreasing (deg) from our control experiments (as in Figure 4). Numbers in parentheses indicate number of genes within the specified category. The majority of overexpressed genes are constant or downward trending, consistent with a delay in degradation of maternal products in histone overexpressing embryos. (B) *abo* underexpressed genes compared to Lott et al. (2011) Many of the underexpressed genes increase over time in WT supporting the idea there is a delay in zygotic transcription in *abo* embryos. Each of the heatmaps were generated by obtaining the median normalized count per gene per nuclear cycle and dividing these values by the maximum median normalized count value for that gene across all nuclear cycles. Thus, each of the cells in the heatmap is the proportion of the maximum normalized count for a given gene per nuclear cycle

Movie 1. Representative *Slbp* embryo with full arrest in NC13
Slbp embryo has slower syncytial blastoderm nuclear cycles and ends the syncytial blastoderm cycles prematurely at NC13. It gastrulates one cell cycle early with about half the number of cells compared to WT. Still images from this movie are represented in Figure 1A. Scale bar represents 50 μm.

Movie 2. Representative *Slbp* embryo partially arrested in NC13
Slbp embryo has slower syncytial blastoderm nuclear cycles and partially arrests at NC13. It gastrulates normally with sections of the embryo in NC13 and NC14. Scale bar represents 50 μm.

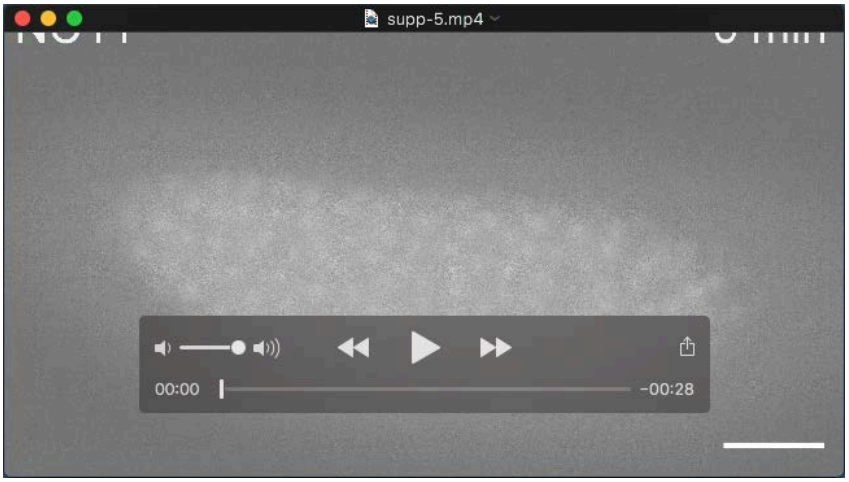

Movie 3. Representative *abo* embryo with extra division
abo embryo has a shortened nuclear cycle 14 and goes on to have a 15th and 16th nuclear cycle before attempting gastrulation. Scale bar represents 50 μm.

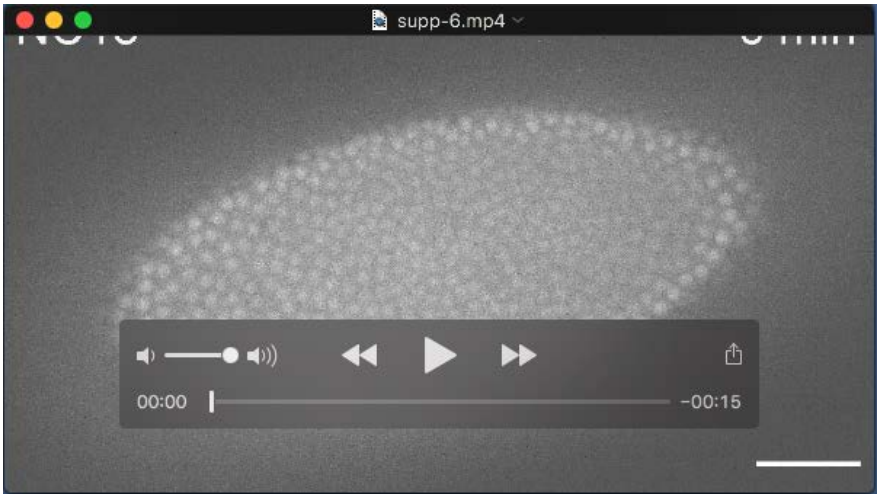

Movie 4. Representative *abo* embryo partially dividing into NC15
abo embryo has a normal NC14 before partially mitosing into NC15. It begins gastrulation while in the process of division and displays ectopic furrow formation. Scale bar represents 50 μm.

Table S1. Syncytial blastoderm phenotypes of histone depletion and overexpression
Range of phenotypes during the syncytial blastoderm stage from *Slbp* and *abo* embryos. The percent of occurrence is noted in the table and total number in parenthesis beside this value. “No nuclei” is defined as no nuclei make it to the embryo’s surface during the course of live imaging which generally occurs ~90 mins after egg laying. “Catastrophic fallout” is defined as fallout which prohibits the embryo from successfully reaching the onset of gastrulation. “NC13” is defined as embryos which initiate their long cell cycle pause at NC13 instead of at NC14. “NC13/14” is defined as embryos which initiated their long cell cycle pause with part of the embryo in NC13 and another in NC14. “NC14” is defined as embryos which go through the syncytial blastoderm stage normally and initiate their cell cycle pause at NC14. “NC14/15” is defined as embryos which undergo a partial extra division before the onset of gastrulation. “NC15” is defined as embryos which undergo a complete extra division before the onset of gastrulation. We excluded from all analysis the ~70% of *Slbp* embryos which have defective blastoderm formation as have been previously reported in *Slbp* mutants and nulls (Sullivan et al., 2001; Iampietro et al., 2014). As previously described the majority of *abo* embryos arrest before the syncytial blastoderm stage (Tomkiel et al., 1991; Tomkiel et al, 1995). We therefore excluded these and *abo* embryos which undergo catastrophic fallout from analysis. However, of the ~40% of embryos that form blastoderm, ~6% do a complete extra division and another ~4% do a partial extra division.

Click here to Download Table S1

Table S2: Differentially expressed gene counts for all genotypes and cell cycles
The number of genes in each category for all differential expression analysis conducted in this manuscript.

Click here to Download Table S2

Table S3: Differentially expressed genes in all *Slbp* to WT comparisons
Table with results from the differential gene expression analysis (using DESeq2) including FDR adjusted p-values that were used to provide significance thresholds for all *Slbp* comparisons.

Click here to Download Table S3

Table S4: Gene lists for differentially expressed genes in all Slbp comparisons
Gene names and identifiers for all genes identified as differentially expressed in *Slbp* at either timepoint.

Click here to Download Table S4

Table S5: Normalized gene counts for *Slbp* and WT at each timepoint
Table with the normalized gene counts for *Slbp* and WT for each timepoint. These values are plotted in Figure 2B and S3D.

Click here to Download Table S5

Table S6: Comparison of previous datasets to differentially expressed genes identified in this study
Number of genes and overlaps in each category of comparison between all differentially expressed genes identified in this study and the Lott et. al (2011), De Renzis et. al. (2007), and Lu et. al (2009) datasets (gene lists for previous datasets included as Table S22). P-values generated by a two-sided Fisher’s exact test. These numbers underlie the overlaps displayed in Figures 2D, 3D, S3E, and S6.

Click here to Download Table S6

Table S7: Differentially expressed genes in *abo* NC14 to WT NC14 comparisons
Table with results from the differential gene expression analysis (using DESeq2) including FDR adjusted p-values that were used to provide significance thresholds for the pooled *abo* comparison.

Click here to Download Table S7

Table S8: Gene lists for differentially expressed genes in *abo* NC14 to WT NC14 comparisons
Gene names and identifiers for all genes identified as differentially expressed for the pooled *abo* datasets.

Click here to Download Table S8

Table S9: Normalized gene counts for *abo* and WT at NC14
Table with the normalized gene counts for *abo* and WT for pooled dataset. These values are plotted in Figures 3B.

Click here to Download Table S9

Table S10: Differentially expressed genes in *abo* timecourse comparisons
Table with results from the differential gene expression analysis (using DESeq2) including FDR adjusted p-values that were utilized to provide significance thresholds for the *abo* timecourse comparison.

Click here to Download Table S10

Table S11: Gene lists for differentially expressed genes in *abo* timecourse comparisons
Gene names and identifiers for all genes identified as differentially expressed in the timecourse *abo* datasets.

Click here to Download Table S11

Table S12: Normalized gene counts for *abo* timecourse
Table with the normalized gene counts for *abo* and WT timecourse dataset. These values are plotted in Figure S5C.

Click here to Download Table S12

Table S13: Transcriptional trajectory of all genes detected between Pre9 to NC14 for the wild-type
Classification of all genes into “transcription”, “flat”, and “degraded” derived from Pre9 vs NC14 comparison in WT as described in figure 4A and Methods.

Click here to Download Table S13

Table S14: Differentially expressed gene distribution compared to WT transcriptional trajectory
Counts from advance gene-category classification representing histone manipulations v/s wild-type differential expression at a given stage compared to the temporal transcriptional profile in wild-type for the same set of genes (see Table 13 and Methods for more details). These numbers are used in Figures 4B and S7.

Click here to Download Table S14

Table S15: Differentially expressed genelist for genes in *Slbp* compared to WT transcriptional trajectory
Gene names and identifiers for all genes identified as differentially expressed in *Slbp* and classified into “transcription”, “flat”, and “degraded” categories derived from Pre9 vs NC14 comparison in WT. The comparisons to WT NC14 are used as the *Slbp* gene list in Figure 4B.
Click here to Download Table S15

Table S16: Differentially expressed genelist for *abo* timecourse compared to WT transcriptional trajectory
Gene names and identifiers for all genes identified as differentially expressed in abo timecourse and classified into “transcription”, “flat”, and “degraded” categories derived from Pre9 vs NC14 comparison in WT. These genes lists are used as the *abo* gene lists in Figures 4B and S7.
Click here to Download Table S16

Table S17: Comparison of modENCODE data and DE genes from *Slbp*
Table with gene numbers, overlaps and Fisher’s exact test results for promoter peaks from different embryonic modENCODE ChIP-seq factors quired for overlap with *Slbp* DE genes belonging to transcriptional categories defined as new transcription, flat, and degradation with appropriate background. These enrichments are plotted in Figue 4B.
Click here to Download Table S17

Table S18: Comparison of modENCODE data and DE genes from *abo* timecourse
Table with gene numbers, overlaps and Fisher’s exact test results for promoter peaks from different embryonic modENCODE ChIP-seq factors quired for overlap with *abo* DE genes belonging to transcriptional categories defined as new transcription, unchanged and degradation with appropriate background. These enrichments are plotted in Figure 4B.
Click here to Download Table S18

Table S19: Effects of thresholds cutoffs on result reproducibility
Table detailing the number of genes in each set for all comparisons with different combinations of p-value and expression fold change cutoffs. Note the marked loss of genes in the WT NC13 to WT NC14 comparison when expression cutoffs are applied.
Click here to Download Table S19

Table S20: Differentially expressed genes are also expressed in WT
Table showing the percent of genes in each comparison that were detected at all in the stage matched WT controls. The vast majority of genes in all comparisons are present in WT, just in different abundance indicating that our results are not the result of genome wide dysregulation.
Click here to Download Table S20

Table S21: Raw and mapped read counts
Table showing the number of raw reads and mapped reads for all datasets generated in this study.
Click here to Download Table S21

Table S22: Gene lists from literature datasets used in this study
Gene lists from Lott et. al (2011), De Renzis et. al (2007), and Lu et. al (2009) used for comparisons in this study. These gene lists underlie the overlaps displayed in Figures 2D, 3D, S3E, and S6.
Click here to Download Table S22

Supplementary Materials and Methods:

RNA collection - single embryo and pooled

Single WT and *Slbp* embryos:
Collections for RNA from single embryos were dechorionated with 4% sodium hypochlorite, washed with DI water, and then mounted in Nunc microwell trays with water (VWR, 470378). Nuclear stage was observed via RFP fluorescence with microscopy settings previously described. Nuclear stage was determined by tracking embryo development as nuclei first surface at nuclear cycle 10. Individual *Slbp* and WT embryos were confirmed to be in the desired nuclear cycle interphase or mitosis. Minimal fallout criteria were established to avoid massive downregulation of zygotic transition observed in *Slbp* mutant and null embryos due to embryonic death (Sullivan et al., 2001; Iampietro et al., 2014; Lefebvre et al., 2016). Embryos that displayed groups of nuclei falling out of the blastoderm surface during the nuclear divisions before collection were discarded. Individual embryos were placed into an RNase free tube, lysed with a sterile needle. Then 100 µl of lysis buffer (Applied Biosystems, KIT0214) was added, and embryos were flash-frozen in liquid nitrogen, and stored at -80°C. Six biological replicates were collected for WT 13 and WT 14. Five biological replicates were collected for *Slbp* NC13.

Individual Pre-NC9 WT and *Slbp* embryos were collected after one-hour laying, confirmed to be preblastoderm stage by visualization in halocarbon oil (Sigma, H8773), and processed as above. Five biological replicates were collected for each genotype.

Single, time course WT and *abo* embryos:
For individual *abo* and WT embryos, each embryo was mounted as described above and observed at the beginning of NC10. We discarded any embryo whose cell cycle times deviated from our standard times by more than 1 minute in any cycle before collection. These stringent conditions mean that we eliminated any *abo* embryo that would have undergone an extra division and that changes in cell cycle times cannot explain differences in gene expression. Individual embryos were placed into an RNase free tube, lysed with a sterile needle. Then 100 µl of lysis buffer (Applied Biosystems, KIT0214) was added, and embryos were flash-frozen in liquid nitrogen, then stored at -80°C. Individual unfertilized WT and *abo* embryos were collected after one-hour laying and processed as above. Three biological replicates were collected for each genotype at each time point.

Pooled WT and *abo* embryos:
Collections for RNA from pooled WT and *abo* embryos were placed under halocarbon oil to determine developmental stage. Embryos between 5 and 15 minutes into nuclear cycle 14 were washed with DI water, dechorionated with 4% sodium hypochlorite, and washed with DI water again. Dechorionated embryos were placed in 100 ul RNAlater (Invitrogen, AM7020) and stored at 4°C. Embryos continued to develop for an additional ~15 minutes in RNAlater that resulted in their final collection time of 15-30 minutes into NC14. When 43, 45, and 45 embryos were collected per genotype for each respective replicate RNALater was removed and 100 ul of lysis buffer was added (Applied Biosystems, KIT02014. Embryos were lysed with a RNase free pestle, flash-frozen in liquid nitrogen, and stored at -80°C. RNA from all single and pooled embryos was isolated using PicoPure RNA Isolation Kit following the manufacturer's protocol (Applied Biosystems, KIT02014).

Quantification and Statistical Analysis

Data pre-processing
We split the barcodes using fastq-multx (1.3.1) and then utilized TrimGalore (0.5.0) using the default options to trim adapters. Trimmed reads were then quantified with Salmon (0.10.2) using the default options and the *Drosophila melanogaster* reference transcriptome (r6.19) obtained from flybase. The reference transcriptome was indexed using Salmon (0.10.2) with the default parameters prior to quantification (Table S21, S5, S9, S12).

Differential gene expression (DE) analysis
The counts generated by Salmon were utilized in DESeq2 (1.20.0) to perform differential gene expression (DE) analysis comparing the "mutants" (*abo* or *Slbp*) to the wild-type per cell cycle. We used an FDR adjusted p-value cutoff $\leqslant 0.05$ to determine significantly DE genes and log2fold-change greater than or less than 0 to assign genes to the significantly differentially over- or under-expressed categories respectively. In cases where multiple sequencing runs were used, the technical replicates (i.e. same library run on different flow-cells), were almost identical as we did not detect any DE genes between these (Fig S3A and C, Fig S4A and C, Fig S5A and B). Thus, we collapsed the technical replicates by summing the read counts prior to DE analysis. We additionally imposed a minimal threshold of detecting at least 1 read in 2 or more samples, after collapsing the technical replicates and prior to performing the DE analysis. To visualize similarities between biological replicates of all samples we used the plotPCA function in DESeq2 to visualize the samples in 2D spanned by their first two principal components (Figures S3A, S4A and S5A). We also plotted the Spearman's rank correlation of the normalized counts as a heatmap to visualize correlations across all samples for a given experiment (Figures S3C, S4C and S5B). We did not detect a substantial difference in the total number of transcripts across different time points in a given experiment (Tables S5,S9,S12 and S21). However, due to degradation of maternal and accumulation of zygotic transcripts, not all transcripts are detected in all timepoints. To determine if the DE genes were maternal, zygotic, dependent on the N/C ratio or time dependent, we tested whether there was a significant overlap between the DE genes and relevant gene lists from literature via a two-sided Fisher's exact test (Table S22). An overlap with a p-value $\leqslant 0.05$ was considered as significant. To visualize the enrichment and de-enrichment of specific factors as a heatmap, we multiplied the log10 p-values by +1 for enrichment (shades of red) and -1 for de-enrichment for plotting (shades of blue) based on the magnitude of the odds ratio (>1 or <1 respectively) in Figures 2D, 3D, S3E and S5. See table S6 for all comparisons.

Advance gene-category classification
To generate a robust set of differentially expressed genes across multiple cell cycles we utilized Fisher's p-value combination method implemented in the metaRNASeq R package (1.0.2), to combine the p-values from all of the independent tests between the mutant and wild-type per cell cycle and generated a global FDR adjusted p-value for each gene across all cell cycles. We then assigned a gene significantly DE if it had a global FDR adjusted p-value $\leqslant 0.05$. Subsequently, we inferred the signs of the p-value combined DE genes by comparing with differentially up or down-regulated genes identified at each cell cycle (Table S3, S7, and S10). We excluded any gene that was identified as significantly DE in the global analysis but were not identified as DE in any of the individual cell cycle. We further excluded all genes DE in the unfertilized embryo comparison from the larger set of DE genes, since these would reflect differences in maternal loading. To further classify whether DE genes were DE in mutants due to excess transcription or degradation as compared to wild-type across time, we identified the genes that were upregulated, down-regulated or unchanged (flat) between NC14 and unfertilized embryo in only the wild-type, based on an FDR adjusted p-value $\leqslant 0.05$ (Table

S13). Any gene that is up-regulated in this window, we classify as “new transcription” and genes down-regulated as “degradation”. These two categories largely meet expectations for gene membership. For instance, we find previously identified zygotic genes (De Renzis et al., 2007; Lott et al., 2011) over represented in the new transcription category. However, our classification is more permissive as transcripts that increase over time are included in the new transcription category regardless of the maternal contribution. We then determined how many of the DE genes (up/ down in mutant v/s wild-type) overlapped with the “new transcription” (trx), “degradation” (deg) and “flat” category of genes across time, as inferred from the wild-type data (Table S14, S15, and S16). Thus, genes that are differentially down-regulated in the mutant v/s wild-type comparison but overlap with “new transcription” category are those that have reduced transcription in the mutant over time as compared to the wild-type. While genes that are differentially up-regulated in the mutant v/s wild-type comparison but overlap with “degradation” category are those with increased stability in the mutant over time relative to the wild-type.

modENCODE comparisons

Chromatin signature identification using modENCODE ChIP-- data enrichment at promoters

To understand if genes belonging to the various DE gene-categories were enriched for other chromatin features, we performed an enrichment analysis using all modENCODE ChIP-seq and ChIP-chip datasets at developmental stages including 0-4h, 0-8h, 0-12h and 0-24h post-fertilization. While the 0-4h developmental stage provides the most appropriate comparison for our experiment, we wanted to make sure that our analysis captured all of the early embryogenesis related chromatin signatures. We converted the ChIP-peak coordinates to dm6 using a perl script provided by flybase for coordinate conversion and further re-annotated these peaks using ChIP-seeker R package (1.16.1), with TSS +/-500bp as being promoters. We subsequently extracted all the genes for which there is any ChIP-peak within the promoter region and performed a gene-set enrichment analysis with genes we identified from the relevant RNA-seq analysis. Enrichment analysis was performed via a two-sided Fisher’s exact test in R with the appropriate gene categories. For example, we compared whether the genes that are underexpressed in a given histone manipulation v/s wild-type but are increasing over time in WT (i.e., *Slbp* or *abo* Under expressed and “new transcription” category as defined above) were enriched for the presence or absence of promoter peaks as compared to a background of all newly transcribed genes. An overlap with an FDR adjusted p-value $\leqslant 0.05$ was considered as significant. To visualize the enrichment and de-enrichment of specific factors as a heatmap, we multiplied the log10 p-values by +1 for enrichment (shades of red) and -1 for de-enrichment for plotting (shades of blue) based on the magnitude of the odds ratio (>1 or <1 respectively) in Figure 4B. See supplemental tables S17 for *Slbp* and S18 for abo comparisons.

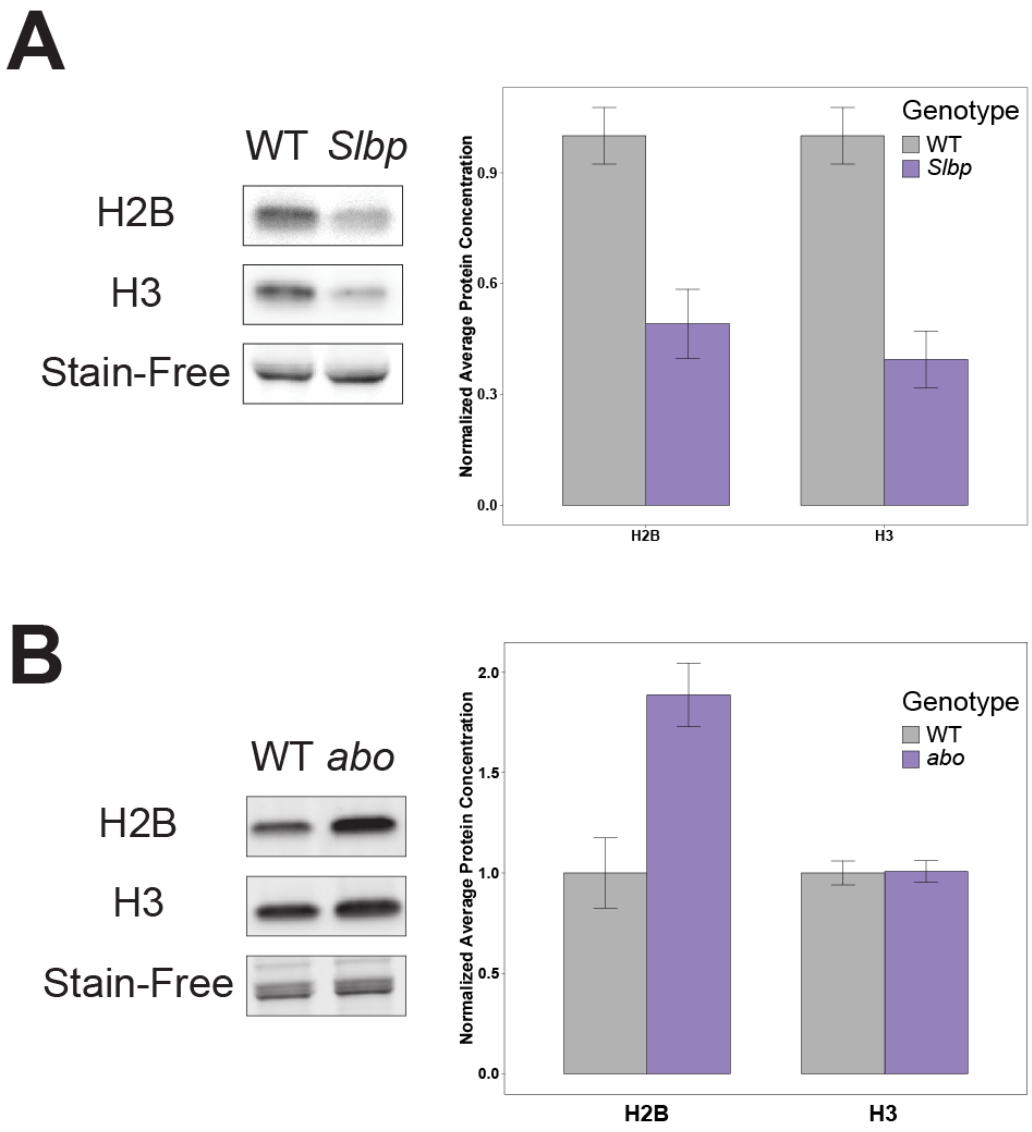

Figure S1. *Slbp* RNAi and *abo* embryos have altered histone protein levels
(A) Total H2B and H3 protein from WT and *Slbp* embryos collected 55 minutes after pole cell formation (early NC14 in WT) from western blotting with 5 embryos per lane. *Slbp* embryos have approximately a ~50% reduction in H2B protein and ~60% reduction in H3 protein (n=3). Bars represent mean and SEM. (B) Total H2B and H3 protein from *abo* embryos at collected 55 minutes after pole cell formation (early NC14 in WT) from western blotting. *abo* embryos have ~90% increase in H2B while total H3 was unchanged between WT (n=5) and *abo* (n=6) embryos. Bars represent mean and SEM. We note that the antibodies used for the assay cannot distinguish between the replication-coupled and replication-independent H3 variants and so the effect size on the replication-coupled H3 may be greater than reported here if there is compensation by the replication-independent variant.

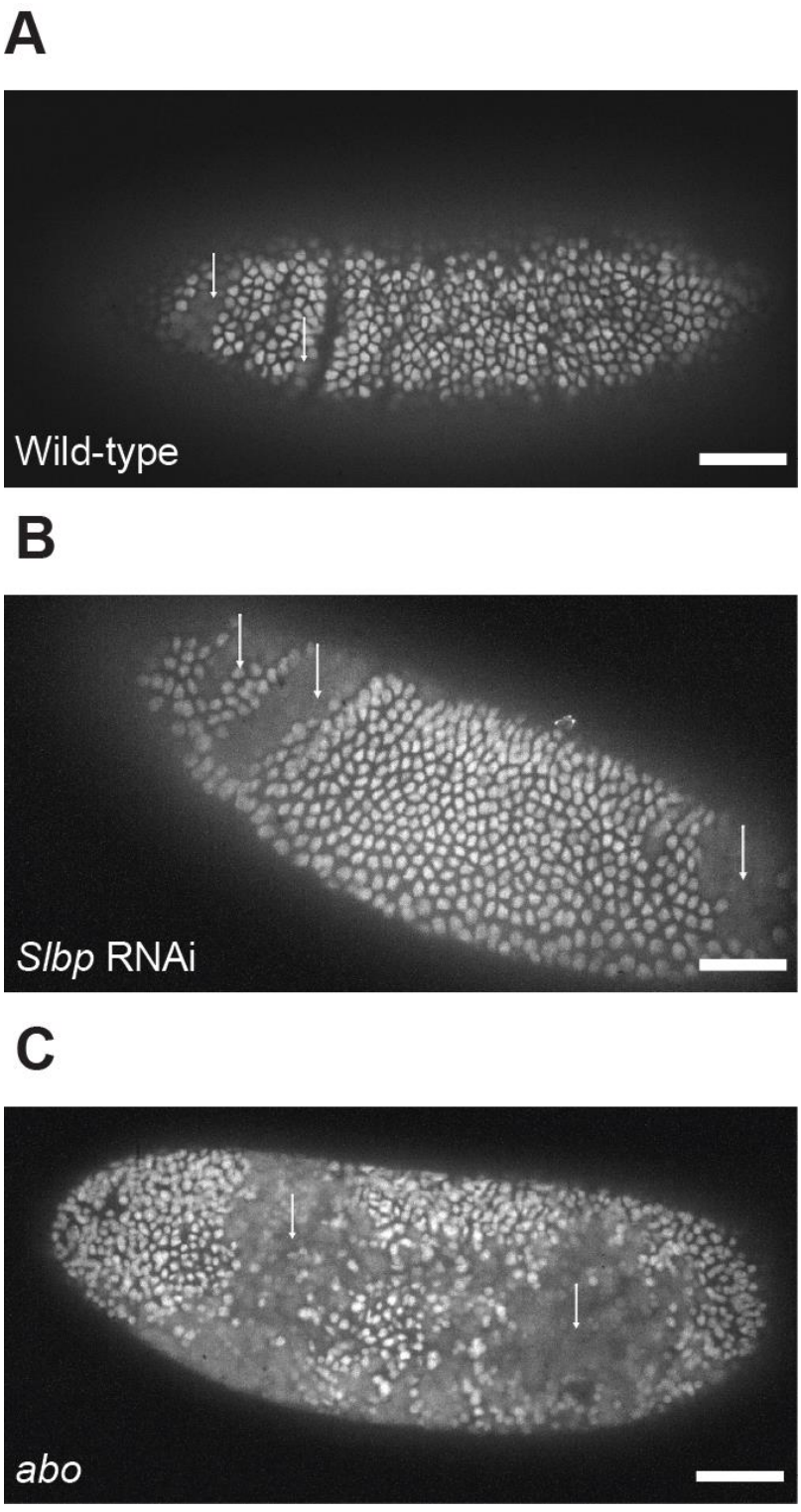

Figure S2. *Slbp* RNAi and *abo* embryos attempt post-MBT development
(A) WT embryo post-MBT after NC14. Mitotic domains and gastrulation movements form normally and with characteristic temporal and spatial dynamics. Arrows indicate mitotic domains. (B) *Slbp* embryo that enters gastrulation in NC13. Mitotic domain formation and gastrulation appear unaffected despite embryos having reduced numbers of cells. These embryos proceed through early-to-mid embryogenesis relatively normally but die before hatching. Arrows indicate mitotic domain formation. (C) *abo* embryos that enters gastrulation in NC15. *abo* embryos that undergo extra divisions still attempt post-MBT behaviors such as mitotic domain formation and gastrulation but are severely disrupted. Arrows indicate aberrant mitotic domain formation. Scale bar represents 50 μm.

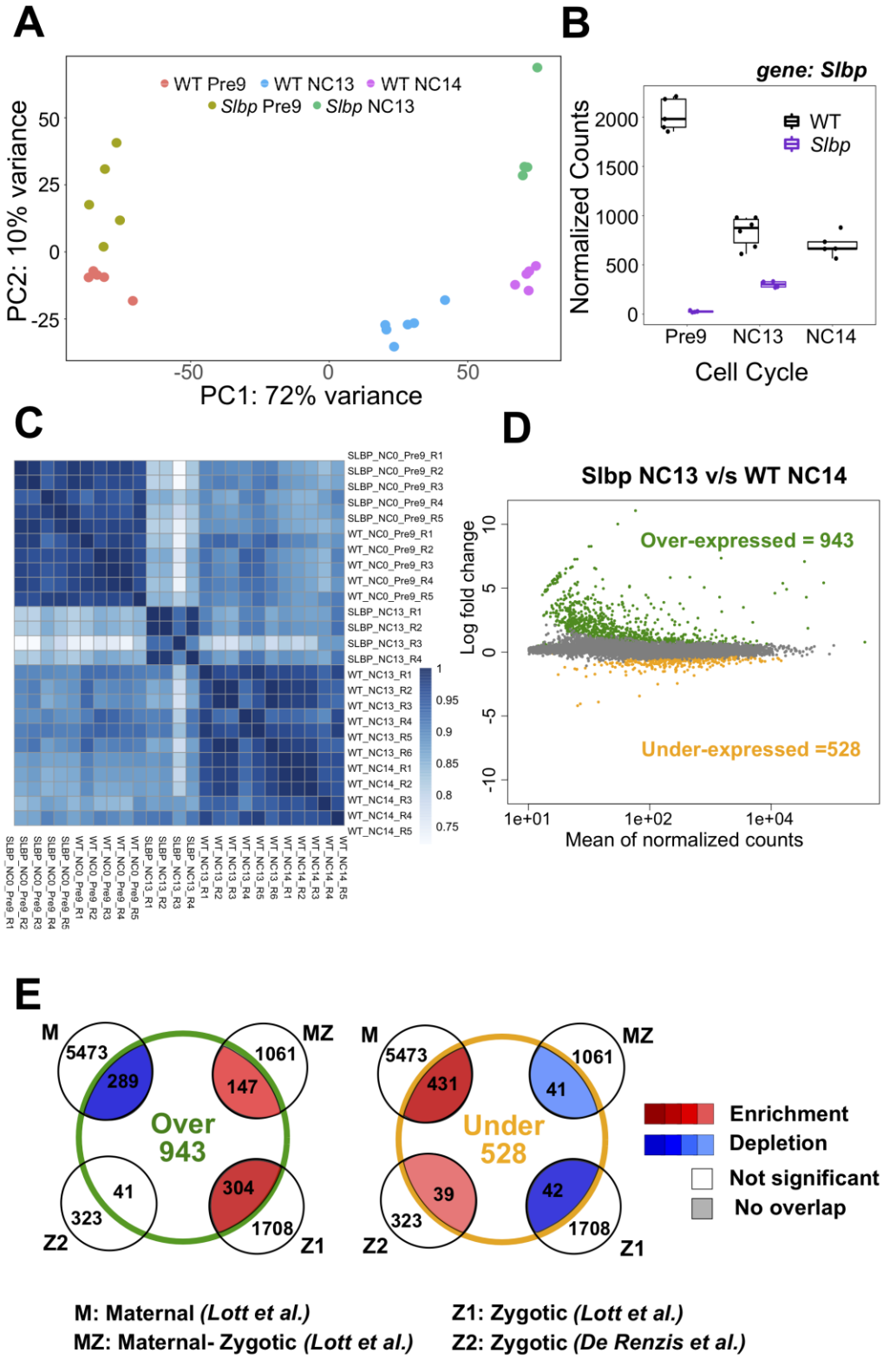

Figure S3. Depletion of maternal histones advance MZT
(A) Principal Components Analysis of *Slbp* and WT expression data demonstrating that global transcriptomic profile is shifted in *Slbp* NC13 as compared WT NC13 and is more similar to WT NC14 indicating that the onset of transcription is advanced in *Slbp* embryos. (B) Normalized counts of *Slbp* mRNA showing a reduction in *Slbp* mutants (n=5 in Pre9 and n=4 in NC13) as compared to WT (n=5 in Pre9, n=6 in NC13 and n=5 in NC14) (C) Spearman's correlation of expression data for WT and *Slbp* embryos at different timepoints. Replicates are more similar to each other than they are to other genotypes and timepoints. (D) When compared to time matched controls (NC14 +20') fewer genes are altered in expression. 943 genes are overexpressed and 528 genes are underexpressed, consistent with premature MZT in the *Slbp* embryos. (E) Data from C compared to previous datasets. Genes overexpressed compared to WT NC14 embryos show enrichment for zygotic transcripts while the underexpressed genes are enriched for maternal transcripts and show a slight enrichment for the De Renzis maternal genes.

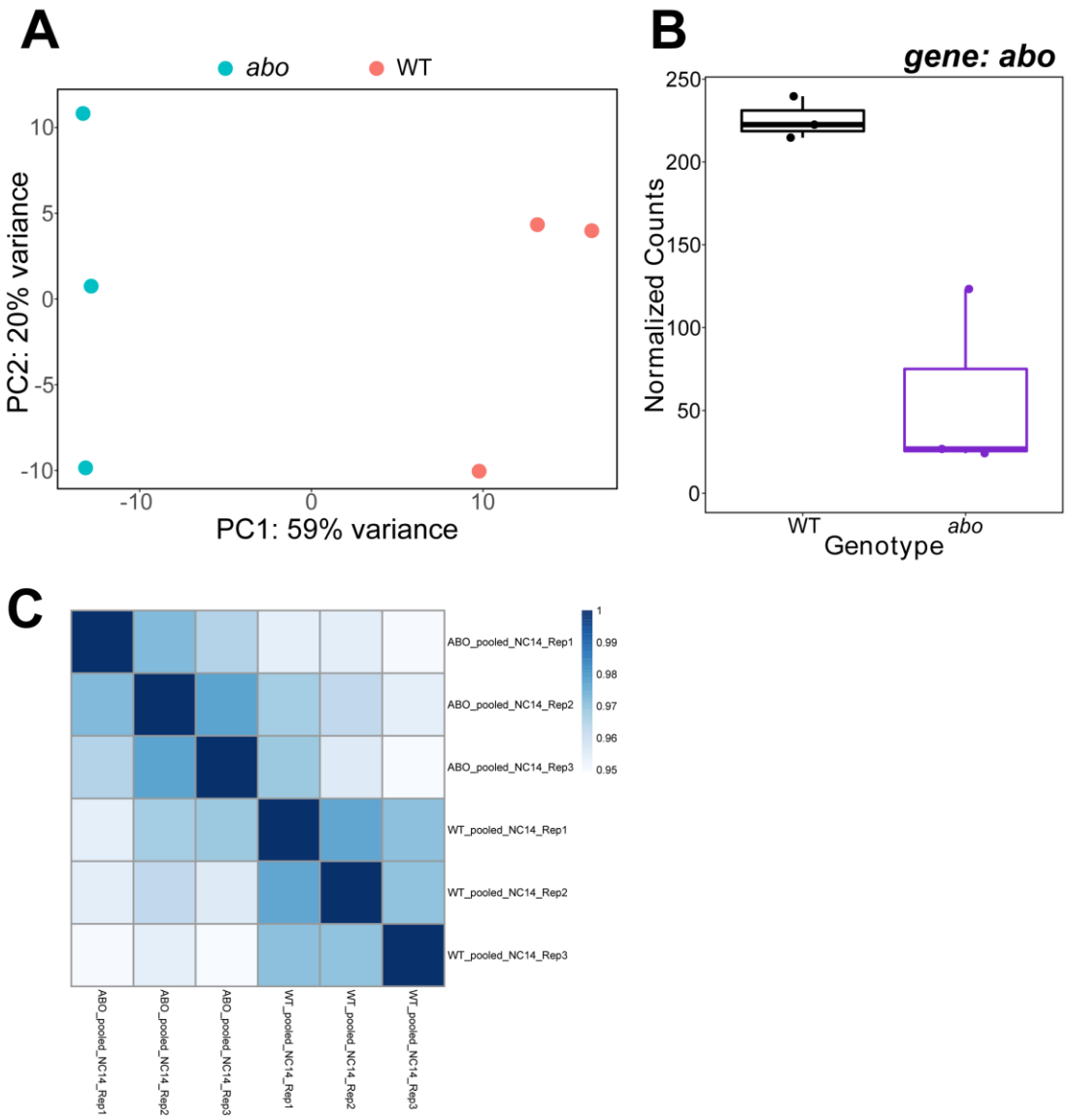

Figure S4. Global transcriptomic differences upon histone overexpression
(A) Principal Components Analysis between the pooled NC14 *abo* and WT expression data showing a clear difference in gene expression between genotypes at this developmental stage. (B) Normalized counts of *abo* mRNA showing reduction in *abo* mutants (n=3) as compared to WT (n=3). (C) Spearman's correlation of expression data for WT and *abo* embryos in NC14.

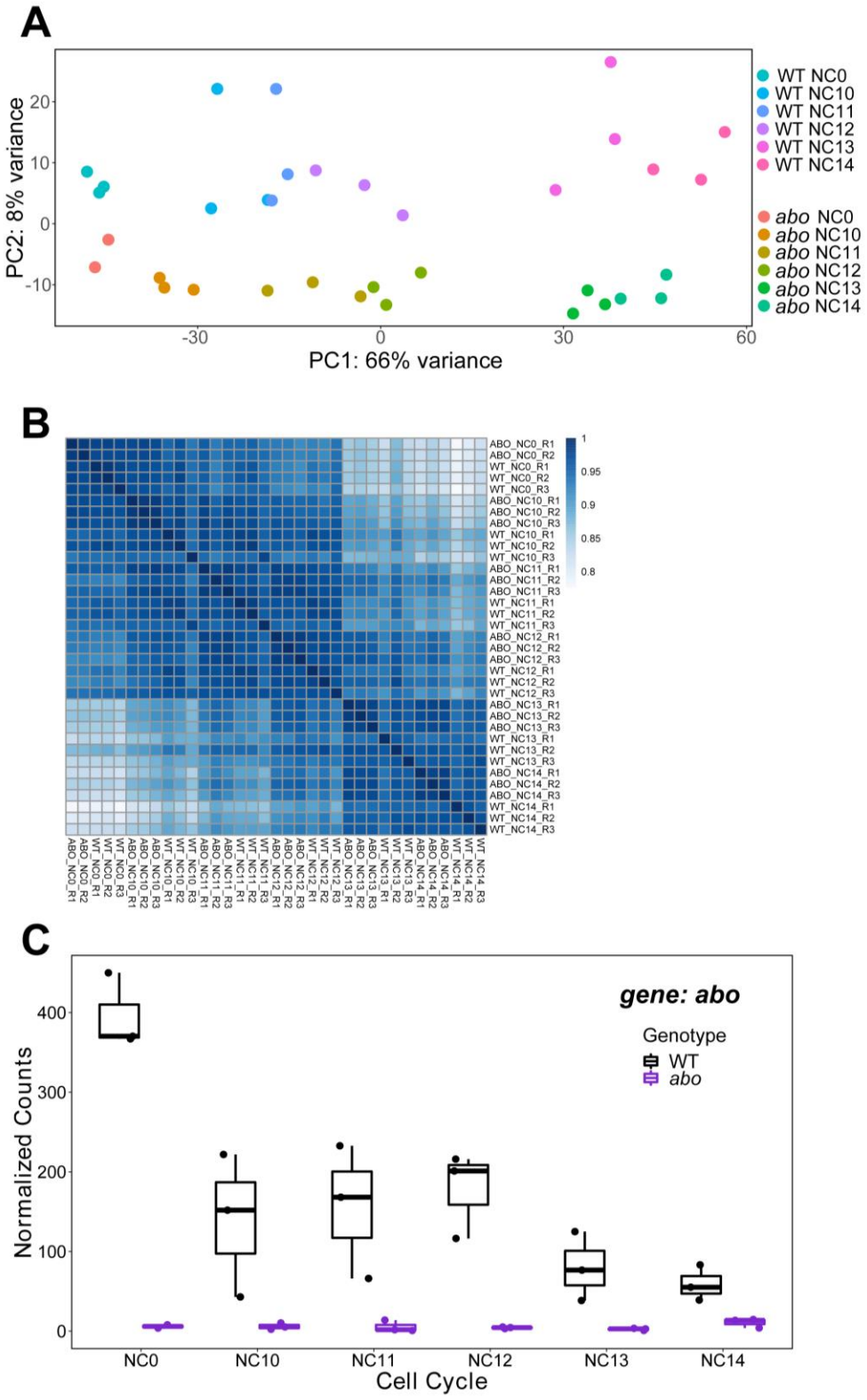

Figure S5. Timecourse transcriptomic differences upon histone overexpression
(A) Principal Components Analysis shows a clear separation across both cell cycle and genotype for the *abo* time-course experiment. (B)Spearman's correlation of expression data for WT and *abo* embryos across all timepoints. (C) Normalized counts of *abo* mRNA showing a reduction in *abo* mutants (n=2 at NC0 and n=3, all other time-points) as compared to WT (n=3, all time-points)

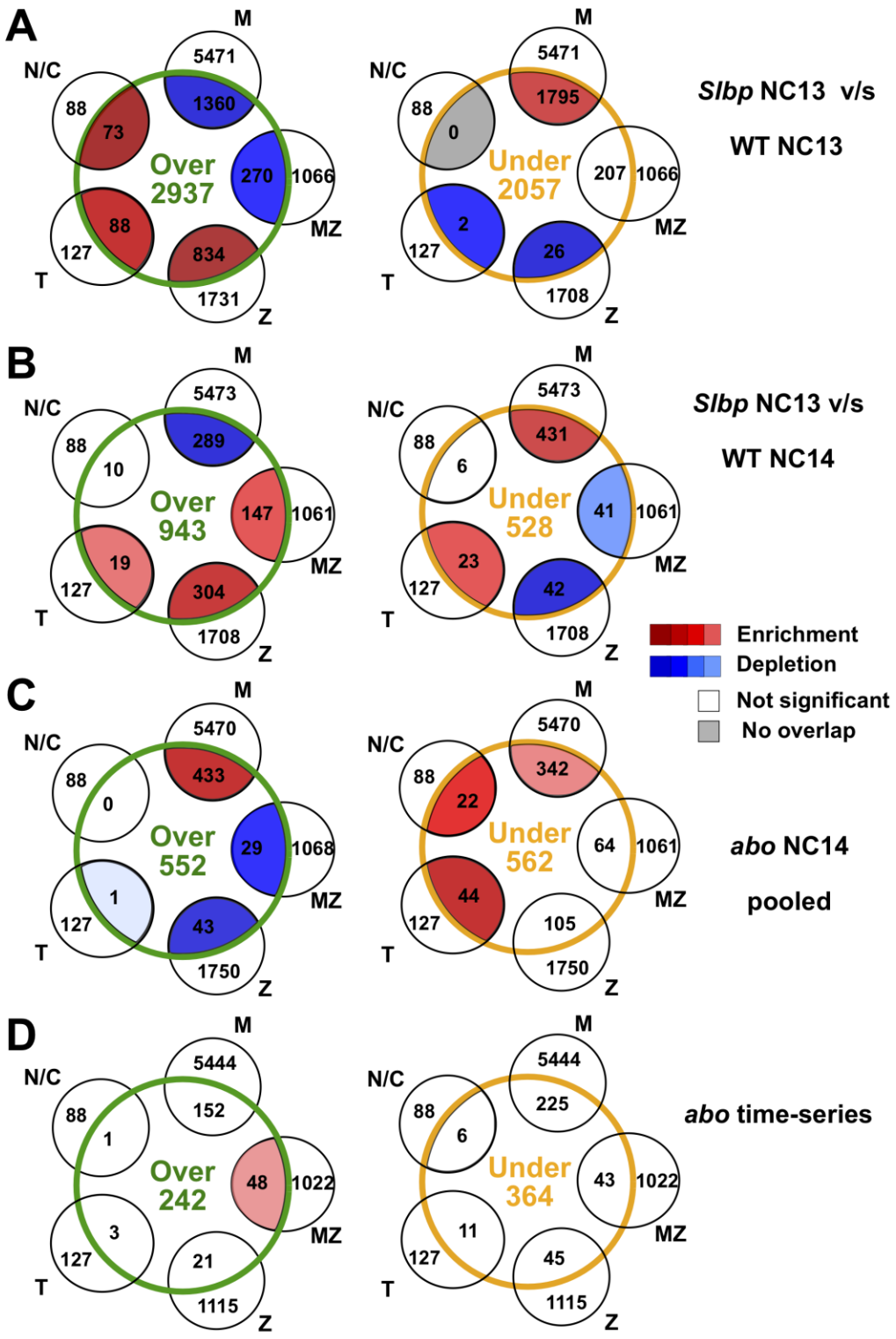

Figure S6. Histone sensitivity changes the onset of ZGA, but cannot explain previous N/C ratio dependent gene sets (A) *Slbp* NC13 compared to WT NC13. Data the same as Figure 2D except the De Renzis et al. (2007) maternal data has been split into N/C and time dependent genes as per Lu et al. (2009). Both N/C and time dependent genes are enriched in the overexpressed and depleted in the underexpressed categories, consistent with global advancement of the MZT. (B) *Slbp* NC13 compared to WT NC14. Data corresponds to Figure S3E. When controlled for time, enrichment of N/C ratio dependent genes is lost and time-dependent genes become enriched in both the over and under expressed gene sets. (C) *abo* NC14 compared to WT NC14. Data corresponds to Figure 3D. Both N/C and time dependent genes are enriched in the underexpressed category consistent with a global delay of ZGA. (D) *abo* time series comparison. Although not statistically significant, both N/C ratio and time dependent genes show an odds ratio >1 indicating these are also trending towards enrichment in the underexpressed gene set. Indeed, when the abo timecourse underexpressed genes are compared to De Renzis et. al (2007) zygotic genes dataset from which the N/C and time gene sets are derived the total zygotic overlap shows significant enrichment (p=9.9e-4) indicating that zygotic genes are better represented in the timecourse abo underexpressed group than the overexpressed set (Table S6).

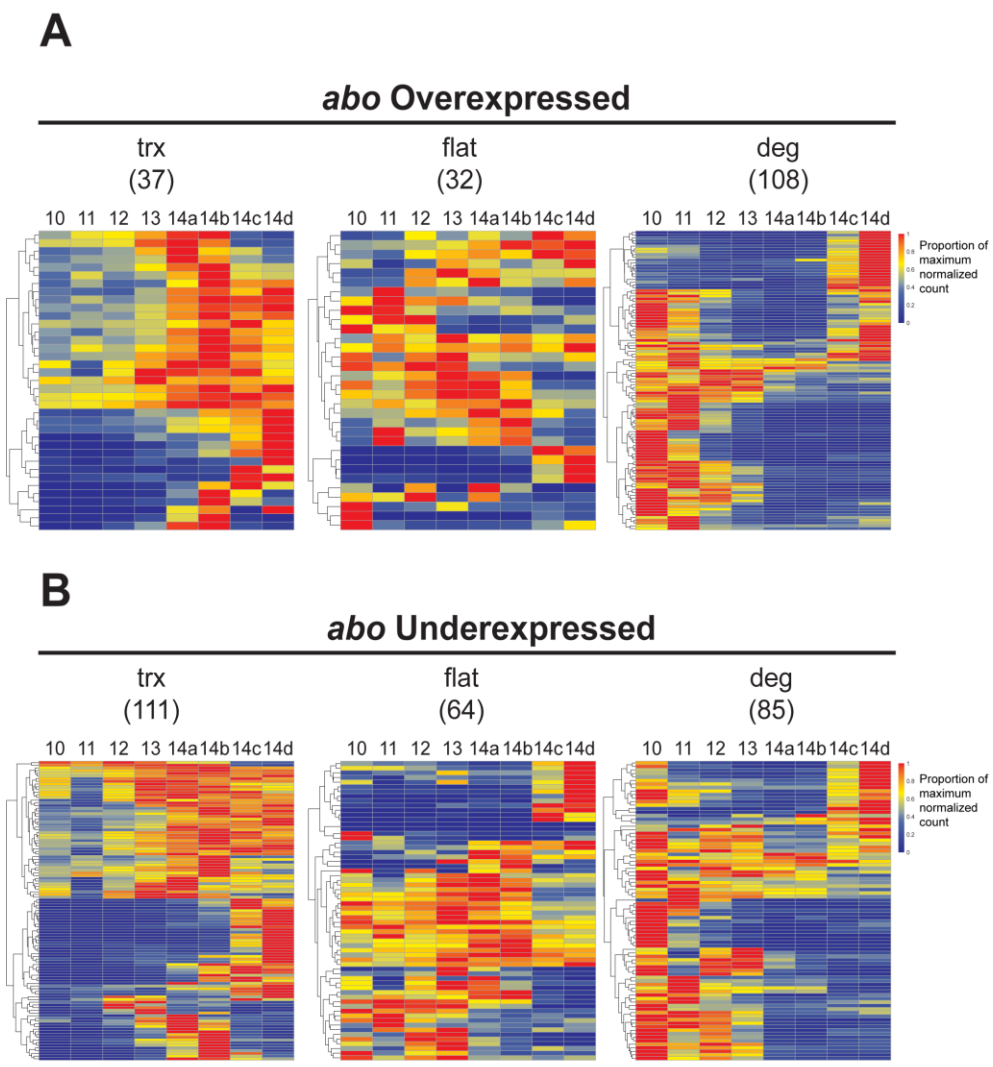

Figure S7. Genes that are knocked down by histone overexpression are expressed during WT MZT

(A) Overexpressed genes in the *abo* time series compared to longer time course from Lott et al. (2011). Each heatmap represents genes categorized as increasing (trx), remaining constant (flat), or decreasing (deg) from our control experiments (as in Figure 4). Numbers in parentheses indicate number of genes within the specified category. The majority of overexpressed genes are constant or downward trending, consistent with a delay in degradation of maternal products in histone overexpressing embryos. (B) *abo* underexpressed genes compared to Lott et al. (2011) Many of the underexpressed genes increase over time in WT supporting the idea there is a delay in zygotic transcription in *abo* embryos. Each of the heatmaps were generated by obtaining the median normalized count per gene per nuclear cycle and dividing these values by the maximum median normalized count value for that gene across all nuclear cycles. Thus, each of the cells in the heatmap is the proportion of the maximum normalized count for a given gene per nuclear cycle

Movie 1. Representative *Slbp* embryo with full arrest in NC13
Slbp embryo has slower syncytial blastoderm nuclear cycles and ends the syncytial blastoderm cycles prematurely at NC13. It gastrulates one cell cycle early with about half the number of cells compared to WT. Still images from this movie are represented in Figure 1A. Scale bar represents 50 µm.

Movie 2. Representative *Slbp* embryo partially arrested in NC13
Slbp embryo has slower syncytial blastoderm nuclear cycles and partially arrests at NC13. It gastrulates normally with sections of the embryo in NC13 and NC14. Scale bar represents 50 µm.

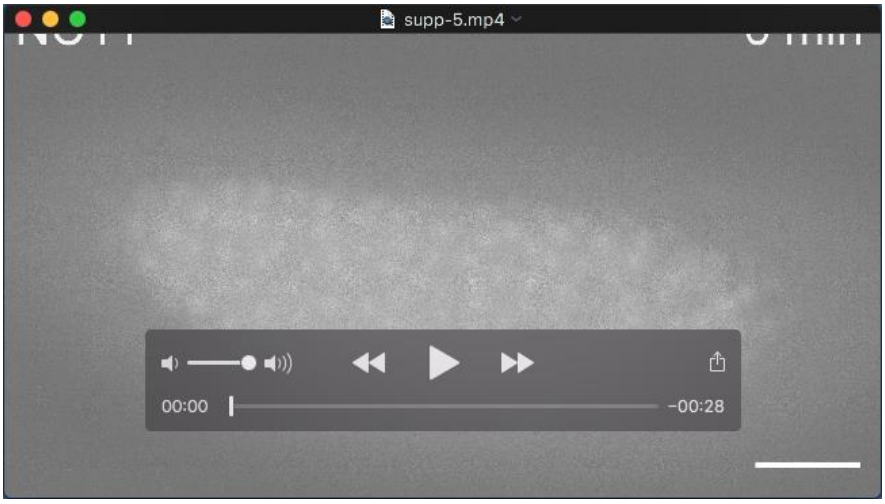

Movie 3. Representative *abo* embryo with extra division
abo embryo has a shortened nuclear cycle 14 and goes on to have a 15th and 16th nuclear cycle before attempting gastrulation. Scale bar represents 50 μm.

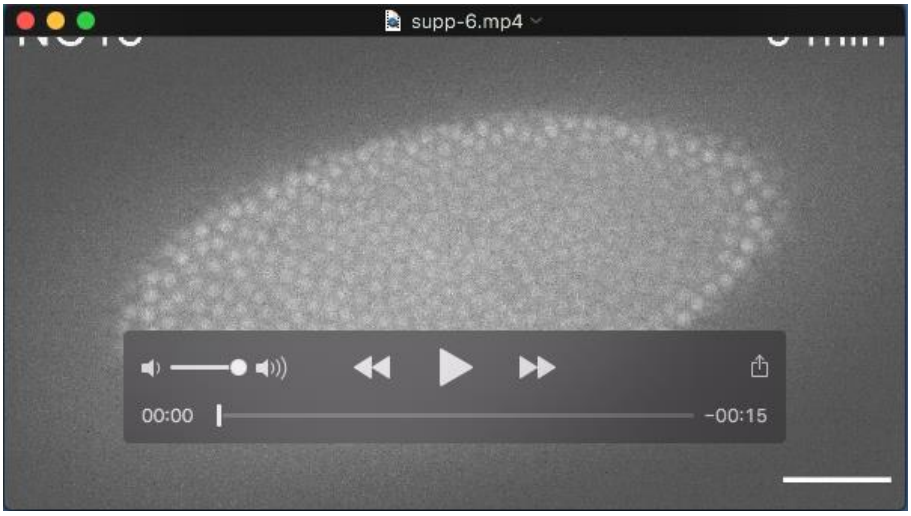

Movie 4. Representative *abo* embryo partially dividing into NC15
abo embryo has a normal NC14 before partially mitosing into NC15. It begins gastrulation while in the process of division and displays ectopic furrow formation. Scale bar represents 50 μm.

Table S1. Syncytial blastoderm phenotypes of histone depletion and overexpression
Range of phenotypes during the syncytial blastoderm stage from *Slbp* and *abo* embryos. The percent of occurrence is noted in the table and total number in parenthesis beside this value. “No nuclei” is defined as no nuclei make it to the embryo’s surface during the course of live imaging which generally occurs ~90 mins after egg laying. “Catastrophic fallout” is defined as fallout which prohibits the embryo from successfully reaching the onset of gastrulation. “NC13” is defined as embryos which initiate their long cell cycle pause at NC13 instead of at NC14. “NC13/14” is defined as embryos which initiated their long cell cycle pause with part of the embryo in NC13 and another in NC14. “NC14” is defined as embryos which go through the syncytial blastoderm stage normally and initiate their cell cycle pause at NC14. “NC14/15” is defined as embryos which undergo a partial extra division before the onset of gastrulation. “NC15” is defined as embryos which undergo a complete extra division before the onset of gastrulation. We excluded from all analysis the ~70% of *Slbp* embryos which have defective blastoderm formation as have been previously reported in *Slbp* mutants and nulls (Sullivan et al., 2001; Iampietro et al., 2014). As previously described the majority of *abo* embryos arrest before the syncytial blastoderm stage (Tomkiel et al., 1991; Tomkiel et al, 1995). We therefore excluded these and *abo* embryos which undergo catastrophic fallout from analysis. However, of the ~40% of embryos that form blastoderm, ~6% do a complete extra division and another ~4% do a partial extra division.

Click here to Download Table S1

Table S2: Differentially expressed gene counts for all genotypes and cell cycles
The number of genes in each category for all differential expression analysis conducted in this manuscript.

Click here to Download Table S2

Table S3: Differentially expressed genes in all *Slbp* to WT comparisons
Table with results from the differential gene expression analysis (using DESeq2) including FDR adjusted p-values that were used to provide significance thresholds for all *Slbp* comparisons.

Click here to Download Table S3

Table S4: Gene lists for differentially expressed genes in all Slbp comparisons
Gene names and identifiers for all genes identified as differentially expressed in *Slbp* at either timepoint.

Click here to Download Table S4

Table S5: Normalized gene counts for *Slbp* and WT at each timepoint
Table with the normalized gene counts for *Slbp* and WT for each timepoint. These values are plotted in Figure 2B and S3D.

Click here to Download Table S5

Table S6: Comparison of previous datasets to differentially expressed genes identified in this study
Number of genes and overlaps in each category of comparison between all differentially expressed genes identified in this study and the Lott et. al (2011), De Renzis et. al. (2007), and Lu et. al (2009) datasets (gene lists for previous datasets included as Table S22). P-values generated by a two-sided Fisher's exact test. These numbers underlie the overlaps displayed in Figures 2D, 3D, S3E, and S6.

Click here to Download Table S6

Table S7: Differentially expressed genes in *abo* NC14 to WT NC14 comparisons
Table with results from the differential gene expression analysis (using DESeq2) including FDR adjusted p-values that were used to provide significance thresholds for the pooled *abo* comparison.

Click here to Download Table S7

Table S8: Gene lists for differentially expressed genes in *abo* NC14 to WT NC14 comparisons
Gene names and identifiers for all genes identified as differentially expressed for the pooled *abo* datasets.

Click here to Download Table S8

Table S9: Normalized gene counts for *abo* and WT at NC14
Table with the normalized gene counts for *abo* and WT for pooled dataset. These values are plotted in Figures 3B.

Click here to Download Table S9

Table S10: Differentially expressed genes in *abo* timecourse comparisons
Table with results from the differential gene expression analysis (using DESeq2) including FDR adjusted p-values that were utilized to provide significance thresholds for the *abo* timecourse comparison.

Click here to Download Table S10

Table S11: Gene lists for differentially expressed genes in *abo* timecourse comparisons
Gene names and identifiers for all genes identified as differentially expressed in the timecourse *abo* datasets.

Click here to Download Table S11

Table S12: Normalized gene counts for *abo* timecourse
Table with the normalized gene counts for *abo* and WT timecourse dataset. These values are plotted in Figure S5C.

Click here to Download Table S12

Table S13: Transcriptional trajectory of all genes detected between Pre9 to NC14 for the wild-type
Classification of all genes into “transcription”, “flat”, and “degraded” derived from Pre9 vs NC14 comparison in WT as described in figure 4A and Methods.

Click here to Download Table S13

Table S14: Differentially expressed gene distribution compared to WT transcriptional trajectory
Counts from advance gene-category classification representing histone manipulations v/s wild-type differential expression at a given stage compared to the temporal transcriptional profile in wild-type for the same set of genes (see Table 13 and Methods for more details). These numbers are used in Figures 4B and S7.

Click here to Download Table S14

Table S15: Differentially expressed genelist for genes in *Slbp* compared to WT transcriptional trajectory
Gene names and identifiers for all genes identified as differentially expressed in *Slbp* and classified into “transcription”, “flat”, and “degraded” categories derived from Pre9 vs NC14 comparison in WT. The comparisons to WT NC14 are used as the *Slbp* gene list in Figure 4B.

Click here to Download Table S15

Table S16: Differentially expressed genelist for *abo* timecourse compared to WT transcriptional trajectory
Gene names and identifiers for all genes identified as differentially expressed in abo timecourse and classified into “transcription”, “flat”, and “degraded” categories derived from Pre9 vs NC14 comparison in WT. These genes lists are used as the *abo* gene lists in Figures 4B and S7.

Click here to Download Table S16

Table S17: Comparison of modENCODE data and DE genes from *Slbp*
Table with gene numbers, overlaps and Fisher's exact test results for promoter peaks from different embryonic modENCODE ChIP-seq factors quired for overlap with *Slbp* DE genes belonging to transcriptional categories defined as new transcription, flat, and degradation with appropriate background. These enrichments are plotted in Figue 4B.

Click here to Download Table S17

Table S18: Comparison of modENCODE data and DE genes from *abo* timecourse
Table with gene numbers, overlaps and Fisher's exact test results for promoter peaks from different embryonic modENCODE ChIP-seq factors quired for overlap with *abo* DE genes belonging to transcriptional categories defined as new transcription, unchanged and degradation with appropriate background. These enrichments are plotted in Figure 4B.

Click here to Download Table S18

Table S19: Effects of thresholds cutoffs on result reproducibility
Table detailing the number of genes in each set for all comparisons with different combinations of p-value and expression fold change cutoffs. Note the marked loss of genes in the WT NC13 to WT NC14 comparison when expression cutoffs are applied.

Click here to Download Table S19

Table S20: Differentially expressed genes are also expressed in WT
Table showing the percent of genes in each comparison that were detected at all in the stage matched WT controls. The vast majority of genes in all comparisons are present in WT, just in different abundance indicating that our results are not the result of genome wide dysregulation.

Click here to Download Table S20

Table S21: Raw and mapped read counts
Table showing the number of raw reads and mapped reads for all datasets generated in this study.

Click here to Download Table S21

Table S22: Gene lists from literature datasets used in this study
Gene lists from Lott et. al (2011), De Renzis et. al (2007), and Lu et. al (2009) used for comparisons in this study. These gene lists underlie the overlaps displayed in Figures 2D, 3D, S3E, and S6.

Click here to Download Table S22

Supplementary Materials and Methods:

RNA collection - single embryo and pooled

Single WT and *Slbp* embryos:
Collections for RNA from single embryos were dechorionated with 4% sodium hypochlorite, washed with DI water, and then mounted in Nunc microwell trays with water (VWR, 470378). Nuclear stage was observed via RFP fluorescence with microscopy settings previously described. Nuclear stage was determined by tracking embryo development as nuclei first surface at nuclear cycle 10. Individual *Slbp* and WT embryos were confirmed to be in the desired nuclear cycle interphase or mitosis. Minimal fallout criteria were established to avoid massive downregulation of zygotic transition observed in *Slbp* mutant and null embryos due to embryonic death (Sullivan et al., 2001; Iampietro et al., 2014; Lefebvre et al., 2017). Embryos that displayed groups of nuclei falling out of the blastoderm surface during the nuclear divisions before collection were discarded. Individual embryos were placed into an RNase free tube, lysed with a sterile needle. Then 100 µl of lysis buffer (Applied Biosystems, KIT0214) was added, and embryos were flash-frozen in liquid nitrogen, and stored at -80°C. Six biological replicates were collected for WT 13 and WT 14. Five biological replicates were collected for *Slbp* NC13.

Individual Pre-NC9 WT and *Slbp* embryos were collected after one-hour laying, confirmed to be preblastoderm stage by visualization in halocarbon oil (Sigma, H8773), and processed as above. Five biological replicates were collected for each genotype.

Single, time course WT and *abo* embryos:
For individual *abo* and WT embryos, each embryo was mounted as described above and observed at the beginning of NC10. We discarded any embryo whose cell cycle times deviated from our standard times by more than 1 minute in any cycle before collection. These stringent conditions mean that we eliminated any *abo* embryo that would have undergone an extra division and that changes in cell cycle times cannot explain differences in gene expression. Individual embryos were placed into an RNase free tube, lysed with a sterile needle. Then 100 µl of lysis buffer (Applied Biosystems, KIT0214) was added, and embryos were flash-frozen in liquid nitrogen, then stored at -80°C. Individual unfertilized WT and *abo* embryos were collected after one-hour laying and processed as above. Three biological replicates were collected for each genotype at each time point.

Pooled WT and *abo* embryos:
Collections for RNA from pooled WT and *abo* embryos were placed under halocarbon oil to determine developmental stage. Embryos between 5 and 15 minutes into nuclear cycle 14 were washed with DI water, dechorionated with 4% sodium hypochlorite, and washed with DI water again. Dechorionated embryos were placed in 100 ul RNAlater (Invitrogen, AM7020) and stored at 4°C. Embryos continued to develop for an additional ~15 minutes in RNAlater that resulted in their final collection time of 15-30 minutes into NC14. When 43, 45, and 45 embryos were collected per genotype for each respective replicate RNALater was removed and 100 ul of lysis buffer was added (Applied Biosystems, KIT02014. Embryos were lysed with a RNase free pestle, flash-frozen in liquid nitrogen, and stored at -80°C. RNA from all single and pooled embryos was isolated using PicoPure RNA Isolation Kit following the manufacturer's protocol (Applied Biosystems, KIT02014).

Quantification and Statistical Analysis

Data pre-processing
We split the barcodes using fastq-multx (1.3.1; Aronesty, 2013) and then utilized TrimGalore (0.5.0) using the default options to trim adapters. Trimmed reads were then quantified with Salmon (0.10.2; Patro et al., 2017) using the default options and the *Drosophila melanogaster* reference transcriptome (r6.19) obtained from flybase. The reference transcriptome was indexed using Salmon (0.10.2; Patro et al., 2017) with the default parameters prior to quantification (Table S21, S5, S9, S12).

Differential gene expression (DE) analysis
The counts generated by Salmon were utilized in DESeq2 (1.20.0; Love et al., 2014) to perform differential gene expression (DE) analysis comparing the "mutants" (*abo* or *Slbp*) to the wild-type per cell cycle. We used an FDR adjusted p-value cutoff $\leqslant 0.05$ to determine significantly DE genes and log2fold-change greater than or less than 0 to assign genes to the significantly differentially over- or under-expressed categories respectively. In cases where multiple sequencing runs were used, the technical replicates (i.e. same library run on different flow-cells), were almost identical as we did not detect any DE genes between these (Fig S3A and C, Fig S4A and C, Fig S5A and B). Thus, we collapsed the technical replicates by summing the read counts prior to DE analysis. We additionally imposed a minimal threshold of detecting at least 1 read in 2 or more samples, after collapsing the technical replicates and prior to performing the DE analysis. To visualize similarities between biological replicates of all samples we used the plotPCA function in DESeq2 to visualize the samples in 2D spanned by their first two principal components (Figures S3A, S4A and S5A). We also plotted the Spearman's rank correlation of the normalized counts as a heatmap to visualize correlations across all samples for a given experiment (Figures S3C, S4C and S5B). We did not detect a substantial difference in the total number of transcripts across different time points in a given experiment (Tables S5,S9,S12 and S21). However, due to degradation of maternal and accumulation of zygotic transcripts, not all transcripts are detected in all timepoints. To determine if the DE genes were maternal, zygotic, dependent on the N/C ratio or time dependent, we tested whether there was a significant overlap between the DE genes and relevant gene lists from literature via a two-sided Fisher's exact test (Table S22). An overlap with a p-value $\leqslant 0.05$ was considered as significant. To visualize the enrichment and de-enrichment of specific factors as a heatmap, we multiplied the log10 p-values by +1 for enrichment (shades of red) and -1 for de-enrichment for plotting (shades of blue) based on the magnitude of the odds ratio (>1 or <1 respectively) in Figures 2D, 3D, S3E and S5. See table S6 for all comparisons.

Advance gene-category classification
To generate a robust set of differentially expressed genes across multiple cell cycles we utilized Fisher's p-value combination method implemented in the metaRNASeq R package (1.0.2; Rau et al., 2014), to combine the p-values from all of the independent tests between the mutant and wild-type per cell cycle and generated a global FDR adjusted p-value for each gene across all cell cycles. We then assigned a gene significantly DE if it had a global FDR adjusted p-value $\leqslant$ 0.05. Subsequently, we inferred the signs of the p-value combined DE genes by comparing with differentially up or down-regulated genes identified at each cell cycle (Table S3, S7, and S10). We excluded any gene that was identified as significantly DE in the global analysis but were not identified as DE in any of the individual cell cycle. We further excluded all genes DE in the unfertilized embryo comparison from the larger set of DE genes, since these would reflect differences in maternal loading. To further classify whether DE genes were DE in mutants due

to excess transcription or degradation as compared to wild-type across time, we identified the genes that were upregulated, down-regulated or unchanged (flat) between NC14 and unfertilized embryo in only the wild-type, based on an FDR adjusted p-value $\leqslant$ 0.05 (Table S13). Any gene that is up-regulated in this window, we classify as "new transcription" and genes down-regulated as "degradation". These two categories largely meet expectations for gene membership. For instance, we find previously identified zygotic genes (De Renzis et al., 2007; Lott et al., 2011) over represented in the new transcription category. However, our classification is more permissive as transcripts that increase over time are included in the new transcription category regardless of the maternal contribution. We then determined how many of the DE genes (up/ down in mutant v/s wild-type) overlapped with the "new transcription" (trx), "degradation" (deg) and "flat" category of genes across time, as inferred from the wild-type data (Table S14, S15, and S16). Thus, genes that are differentially down-regulated in the mutant v/s wild-type comparison but overlap with "new transcription" category are those that have reduced transcription in the mutant over time as compared to the wild-type. While genes that are differentially up-regulated in the mutant v/s wild-type comparison but overlap with "degradation" category are those with increased stability in the mutant over time relative to the wild-type.

modENCODE comparisons

Chromatin signature identification using modENCODE ChIP-- data enrichment at promoters

To understand if genes belonging to the various DE gene-categories were enriched for other chromatin features, we performed an enrichment analysis using all modENCODE ChIP-seq and ChIP-chip datasets at developmental stages including 0-4h, 0-8h, 0-12h and 0-24h post-fertilization (modENCODE Consortium et al., 2009). While the 0-4h developmental stage provides the most appropriate comparison for our experiment, we wanted to make sure that our analysis captured all of the early embryogenesis related chromatin signatures. We converted the ChIP-peak coordinates to dm6 using a perl script provided by flybase for coordinate conversion and further re-annotated these peaks using ChIP-seeker R package (1.16.1; Yu et al., 2015), with TSS +/-500bp as being promoters. We subsequently extracted all the genes for which there is any ChIP-peak within the promoter region and performed a gene-set enrichment analysis with genes we identified from the relevant RNA-seq analysis. Enrichment analysis was performed via a two-sided Fisher's exact test in R with the appropriate gene categories. For example, we compared whether the genes that are underexpressed in a given histone manipulation v/s wild-type but are increasing over time in WT (i.e., *Slbp* or *abo* Under expressed and "new transcription" category as defined above) were enriched for the presence or absence of promoter peaks as compared to a background of all newly transcribed genes. An overlap with an FDR adjusted p-value $\leqslant$ 0.05 was considered as significant. To visualize the enrichment and de-enrichment of specific factors as a heatmap, we multiplied the log10 p-values by +1 for enrichment (shades of red) and -1 for de-enrichment for plotting (shades of blue) based on the magnitude of the odds ratio (>1 or <1 respectively) in Figure 4B. See supplemental tables S17 for *Slbp* and S18 for abo comparisons.

Supplementary References

Aronesty, E. (2013). Comparison of sequencing utility programs. *The Open Bioinformatics Journal* 7, 1-8. doi:10.2174/1875036201307010001

Iampietro, C., Bergalet, J., Wang, X., Cody, N. A. L., Chin, A., Lefebvre, F. A., Douziech, M., Krause, H. M. and Lécuyer, E. (2014). Developmentally Regulated Elimination of Damaged Nuclei Involves a Chk2-Dependent Mechanism of mRNA Nuclear Retention. *Dev. Cell* 29, 468-481. doi:10.1016/j.devcel.2014.03.025

Lefebvre, F. A., Benoit Bouvrette, L. P., Bergalet, J. and Lécuyer, E. (2017). Biochemical Fractionation of Time-Resolved Drosophila Embryos Reveals Similar Transcriptomic Alterations in Replication Checkpoint and Histone mRNA Processing Mutants. *J. Mol. Biol*. 429, 3264-3279. doi:10.1016/j.jmb.2017.01.022

Love, M. I., Huber, W. and Anders, S. (2014). Moderated estimation of fold change and dispersion for RNA-seq data with DESeq2. *Genome Biology* 15,

modENCODE Consortium, Celniker, S. E., Dillon, L. A. L., Gerstein, M. B., Gunsalus, K. C., Henikoff, S., Karpen, G. H., Kellis, M., Lai, E. C., Lieb, J. D., et al. (2009). Unlocking the secrets of the genome. *Nature* 459, 927-930. doi:10.1038/459927a

Patro, R., Duggal, G., Love, M. I., Irizarry, R. A. and Kingsford, C. (2017). Salmon provides fast and bias-aware quantification of transcript expression. *Nat. Methods* 14, 417-419. doi:10.1038/nmeth.4197

Rau, A., Marot, G. and Jaffrézic, F. (2014). Differential meta-analysis of RNA-seq data from multiple studies. *BMC Bioinformatics* 15, 91. doi:10.1186/1471-2105-15-91

Sullivan, E., Santiago, C., Parker, E. D., Dominski, Z., Yang, X., Lanzotti, D. J., Ingledue, T. C., Marzluff, W. F. and Duronio, R. J. (2001). Drosophila stem loop binding protein coordinates accumulation of mature histone mRNA with cell cycle progression. *Genes Dev*. 15, 173-187. doi:10.1101/gad.862801

Tomkiel, J., Pimpinelli, S. and Sandler, L. (1991). Rescue from the abnormal oocyte maternal-effect lethality by ABO heterochromatin in Drosophila melanogaster. *Genetics* 128, 583-594.

Tomkiel, J., Fanti, L., Berloco, M., Spinelli, L., Tamkun, J. W., Wakimoto, B. T. and Pimpinelli, S. (1995). Developmental genetical analysis and molecular cloning of the abnormal oocyte gene of Drosophila melanogaster. *Genetics* 140, 615-627.

Yu, G., Wang, L.-G. and He, Q.-Y. (2015). ChIPseeker: an R/Bioconductor package for ChIP peak annotation, comparison and visualization. *Bioinformatics* 31, 2382-2383. doi:10.1093/bioinformatics/btv145